



## Exploring DMS oxidation and implications for global aerosol radiative forcing

Ka Ming Fung<sup>1</sup>, Colette L. Heald<sup>1,2</sup>, Jesse H. Kroll<sup>1</sup>, Siyuan Wang<sup>3</sup>, Duseong S. Jo<sup>4</sup>, Andrew Gettelman<sup>4</sup>, Zheng Lu<sup>5</sup>, Xiaohong Liu<sup>5</sup>, Rahul A. Zaveri<sup>6</sup>, Eric Apel<sup>4</sup>, Donald R. Blake<sup>7</sup>, Jose-Luis Jimenez<sup>8</sup>, Pedro Campuzano-Jost<sup>8</sup>, Patrick Veres<sup>3</sup>, Timothy S. Bates<sup>9</sup>, John E. Shilling<sup>10</sup>, Maria Zawadowicz<sup>11</sup>

<sup>1</sup> Department of Civil and Environmental Engineering, Massachusetts Institute of Technology, Cambridge, MA, USA

<sup>2</sup> Department of Earth, Atmospheric and Planetary Sciences, Massachusetts Institute of Technology, Cambridge, MA, USA

10 <sup>3</sup> Chemical Sciences Laboratory, National Oceanic and Atmospheric Administration, Boulder, CO, USA

<sup>4</sup> Atmospheric Chemistry Observations and Modeling Laboratory, National Center for Atmospheric Research, Boulder, CO, USA

<sup>5</sup> Department of Atmospheric Sciences, Texas A&M University, College Station, TX, USA

<sup>6</sup> Pacific Northwest National Laboratory, Richland, WA, USA

15 <sup>7</sup> Department of Chemistry, University of California, Irvine, CA, USA

<sup>8</sup> Department of Chemistry & Cooperative Institute for Research in Environmental Sciences, University of Colorado, Boulder, CO, USA

<sup>9</sup> The Cooperative Institute for Climate, Ocean, and Ecosystem Studies, College of the Environment, University of Washington, Seattle, WA, USA

20 <sup>10</sup> Atmospheric Sciences and Global Change Division, Pacific Northwest National Laboratory, Richland, WA, USA

<sup>11</sup> Environmental and Climate Sciences Department, Brookhaven National Laboratory, Upton, NY, USA

*Corresponding to:* Ka Ming Fung (kamingfung@mit.edu) & Colette L. Heald (heald@mit.edu)



25 **Abstract.** Aerosol indirect radiative forcing (IRF), which characterizes how aerosols alter cloud  
formation and properties, is very sensitive to the preindustrial (PI) aerosol burden. Dimethyl sulfide  
(DMS), emitted from the ocean, is a dominant natural precursor of non-sea-salt sulfate in the PI and  
pristine present-day (PD) atmospheres. Here we revisit the atmospheric oxidation chemistry of DMS,  
particularly under pristine conditions, and its impact on aerosol IRF. Based on previous laboratory  
30 studies, we expand the simplified DMS oxidation scheme used in the Community Atmospheric Model  
version 6 with chemistry (CAM6-chem) to capture the OH-addition pathway as well as the H-  
abstraction pathway and the associated isomerization branch. These additional oxidation channels of  
DMS produce several stable intermediate compounds, e.g., methanesulfonic acid (MSA) and  
hydroperoxymethyl thioformate (HPMTF), delay the formation of sulfate, and hence, alter the spatial  
35 distribution of sulfate aerosol and radiative impacts. The expanded scheme improves the agreement  
between modeled and observed concentrations of DMS, MSA, HPMTF, and sulfate over most marine  
regions based on the NASA Atmospheric Tomography (ATom), the Aerosol and Cloud Experiments  
in the Eastern North Atlantic (ACE-ENA), and the VAMOS Ocean-Cloud-Atmosphere-Land Study  
Regional Experiment (VOCALS-REx) measurements. We find that the global HPMTF burden, as well  
40 as the burden of sulfate produced from DMS oxidation are relatively insensitive to the assumed  
isomerization rate, but the burden of HPMTF is very sensitive to a potential additional cloud loss. We  
find that global sulfate burden under PI and PD emissions increase to 412 Gg-S (+29%) and 582 Gg-S  
(+8.8%), respectively, compared to the standard simplified DMS oxidation scheme. The resulting  
annual mean global PD direct radiative effect of DMS-derived sulfate alone is  $-0.11 \text{ W m}^{-2}$ . The  
45 enhanced PI sulfate produced via the gas-phase chemistry updates alone dampens the aerosol IRF as  
anticipated ( $-2.2 \text{ W m}^{-2}$  in standard versus  $-1.7 \text{ W m}^{-2}$  with updated gas-phase chemistry). However,  
high clouds in the tropics and low clouds in the Southern Ocean appear particularly sensitive to the  
additional aqueous-phase pathways, counteracting this change ( $-2.3 \text{ W m}^{-2}$ ). This study confirms the  
sensitivity of aerosol IRF to the PI aerosol loading, as well as the need to better understand the processes  
50 controlling aerosol formation in the PI atmosphere and the cloud response to these changes.



## 1 Introduction

The IPCC AR5 (Myhre et al., 2013) indicates that atmospheric aerosol particles are a dominant source of uncertainty in global climate forcing. Aerosols interact with incoming and outgoing radiation directly (via scattering and absorption) and indirectly (via changing cloud properties and lifetime). In particular, the aerosol indirect radiative forcing (IRF) via interactions with clouds is driven by the fractional enhancement of aerosol burden from a preindustrial (PI; 1850) atmosphere to a present-day (PD; 2000) one, with a cleaner PI atmosphere producing a larger IRF (Menon et al., 2002). Carslaw et al. (2013) confirm that the estimated uncertainty in aerosol IRF is dominated by uncertainty in natural aerosols. It is therefore critically important to accurately determine the formation of natural aerosols and their radiative impacts in both PD and PI atmosphere.

Marine dimethyl sulfide (DMS:  $\text{CH}_3\text{SCH}_3$ ) accounts for >50% of natural gas-phase sulfur emissions (Chin et al., 1996; Andreae, 1990; Kilgour et al., 2021). Once emitted into the troposphere, oxidation of DMS takes place within 1–2 days, forming other sulfur-containing products such as sulfuric acid ( $\text{H}_2\text{SO}_4$ ) and methane sulfonic acid (MSA:  $\text{CH}_3\text{SO}_3\text{H}$ ) (Boucher et al., 2003; Breider et al., 2010). These gaseous products can facilitate the formation of new particles as well as cloud condensation nuclei (CCN), especially in the marine boundary layer (MBL) (Charlson et al., 1987; von Glasow and Crutzen, 2004; Kulmala et al., 2000). Sulfate and MSA formed in particle-phase can directly impact the size distribution of aerosols and alter cloud microphysics (Kaufman and Tanré, 1994). DMS is estimated to be responsible for up to 11–18% of global sulfate burden in PD (Yang et al., 2017; Gondwe et al., 2003) and >48% of atmospheric sulfur burden in PI (Tilmes et al., 2019). Though the crucial role of DMS oxidation as a source of natural aerosols has been acknowledged for decades, its oxidation mechanisms are still not well understood (Barnes et al., 2006; Hoffmann et al., 2016).

Global/regional models often simplify the DMS oxidation processes for the sake of computational costs. For example, the Community Atmosphere Model with chemistry (CAM-chem) includes only the oxidation of DMS by OH and  $\text{NO}_3$  radicals, directly producing  $\text{SO}_2$ , which further



oxidizes to produce sulfate (Emmons et al., 2020; Lamarque et al., 2012). This simplification ignores some potentially important reaction intermediates and pathways. For instance, previous studies suggest  
80 that BrO contributes up to 30% of the DMS sink in remote MBL (Boucher et al., 2003; Breider et al., 2010; von Glasow and Crutzen, 2004; Khan et al., 2016). MSA has been found to form efficiently via the multi-phase OH-addition DMS oxidation pathway followed by reaction with OH<sub>(aq)</sub> to form sulfate aerosol in the MBL (von Glasow and Crutzen, 2004; Milne et al., 1989; Zhu et al., 2006). Recently, both theoretical and laboratory studies have proposed that a pristine environment favors the H-  
85 abstraction reaction when DMS is oxidized by OH, generating methylthiomethylperoxy radicals (MSP: CH<sub>3</sub>SCH<sub>2</sub>OO), which further undergoes a series of rapid intramolecular H-shift isomerization reactions, yielding a stable intermediate hydroperoxymethyl thioformate (HPMTF: HOOCH<sub>2</sub>SCHO) (Wu et al., 2015; Berndt et al., 2019). Recent in situ measurements report HPMTF concentrations that equal or even exceed DMS concentrations in the MBL during the day, confirming the importance of the  
90 isomerization branch for capturing the fate of oxidized DMS (Veres et al., 2020; Vermeuel et al., 2020).

The lifetimes of stable intermediates from DMS oxidation can be up to days. As a result, these intermediates can delay the formation of DMS-derived sulfate, affecting not only the spatial distribution of sulfate aerosols but also the effective sulfate yield from DMS as unreacted sulfate precursors may be subject to physical removal through wet or dry deposition. Thus, neglecting these intermediates could  
95 lead to misrepresentation of the spatial distribution of sulfate aerosol loading and limit our ability to accurately determine aerosol radiative forcing.

Here, we implement a more detailed multi-generational and multi-phase chemical mechanism to describe DMS oxidation within the Community Atmosphere Model version 6 with chemistry (CAM6-chem) (Emmons et al., 2020) – the atmosphere component of the Community Earth System  
100 Model version 2.1 (CESM2.1) (Danabasoglu et al., 2020). The expanded chemistry captures the formation of stable intermediates such as MSA and HPMTF alongside SO<sub>2</sub>. We perform multiple sensitivity tests to investigate how the uncertainty in modeling the newly confirmed HPMTF could influence the DMS chemistry and the resulting atmospheric sulfate burden. The model results are compared against an array of in situ observations. Finally, we examine how the natural aerosol



105 background from DMS oxidation simulated with the modified model impacts estimates of aerosol  
radiative forcing.

## 2 Model description

CESM2.1 consists of model components that quantitatively describe the atmosphere, land, sea-  
110 ice, land-ice, rivers, and ocean (Danabasoglu et al., 2020). Fluxes and state variables are exchanged  
through a coupler to describe the co-evolution of these earth system components. Here, we run with a  
coupled atmosphere (CAM6-chem) and land (Community Land Model, CLM5) and use prescribed data  
for the remaining earth system components. In particular, sea surface temperature (SST) and sea ice  
conditions (Hurrell et al., 2008), as well as the mixing ratios of greenhouse gases (Meinshausen et al.,  
115 2017) are all fixed to present-day conditions. Following similar practices in previous studies (Gettelman,  
2015; Gettelman et al., 2019), this configuration aims to constrain the potential environmental  
feedbacks such that the aerosol effects (on atmospheric composition, cloud, and radiation) are due to  
the change in emissions and chemistry only.

### 2.1 Model configuration

120 In this work, CAM6-chem is run in an online configuration with free dynamics at  $1.9^\circ \times 2.5^\circ$   
(latitude by longitude) horizontal resolution and 32 vertical layers (surface to 3 hPa or  $\sim 45$  km), with a  
model timestep of 30 minutes. The default chemistry scheme is Model of Ozone and Related chemical  
Tracers with representations of both tropospheric and stratospheric chemistry (MOZART-TS1)  
(Emmons et al., 2020) with a Volatility Basis Set (VBS) scheme specifically for the gas-phase  
125 intermediate semi-volatile organic precursors of secondary organic aerosols (SOA) (Tilmes et al., 2019).  
The DMS chemistry is described in further detail in **Sect. 2.3**. Aerosols are simulated using the Modal  
Aerosol Model with four modes (MAM4) (Liu et al., 2016) coupled with Model for Simulating Aerosol  
Interactions and Chemistry (MOSAIC) (Zaveri et al., 2008, 2021; Lu et al., 2021), for sulfate ( $\text{SO}_4^{2-}$ ),  
ammonium ( $\text{NH}_4^+$ ), nitrate ( $\text{NO}_3^-$ ), primary organic matters (POM), SOA, sea salt, and mineral dust.



130 MAM4 classifies aerosols into three size-dependent modes (Aitken, accumulation, and coarse) with an  
additional primary carbon mode for handling the aging of fine POM and black carbon (BC). Size  
distributions of aerosols in each mode are assumed to be log-normal with fixed geometric standard  
deviations and varying mode dry or wet radius depending on particle number and changes in total dry  
or wet volume (Liu et al., 2012). MAM4 defines the cut-off size ranges of 0.015–0.053  $\mu\text{m}$  for aerosol  
135 in Aitken mode, 0.058–0.27  $\mu\text{m}$  for accumulation mode, and 0.80–3.65  $\mu\text{m}$  for coarse mode. Dynamic  
partitioning of  $\text{H}_2\text{SO}_4$ ,  $\text{HNO}_3$ ,  $\text{HCl}$ , and  $\text{NH}_3$  to each mode, related particle-phase thermodynamics, as  
well as water content and pH of interstitial aerosols, are computed using the MOSAIC module (Zaveri  
et al., 2008, 2021; Lu et al., 2021). Further details describing the dry and wet deposition, aerosol optical  
properties, radiative transfer, and aerosol-cloud microphysics are described in **Supplementary**  
140 **Information**; these processes are all based on the standard CAM6-chem.

We perform four sets of simulations for the PD and PI atmospheric conditions with the standard  
and our modified chemical schemes. Details of the runs are tabulated in **Table 1**. Each run is performed  
for 10 years with the first year as spin-up and averages over the latter nine years are presented in our  
results.

145

**Table 1.** Configuration of key simulation cases in this study

Case Alias	Chemistry	Anthropogenic Emissions
STD_2000	TS1 with the model-default DMS oxidation reactions in	2000-level
STD_1850	<b>Table 3</b>	1850-level
MOD_2000	TS1 with the new gas-phase and aqueous-phase reactions	2000-level
MOD_1850	in <b>Table 4</b> , <b>Table 5</b> , <b>Table 6</b> , and <b>Table 7</b> .	1850-level
MOD_RE_2000		2000-level



---

MOD_RE_1850	TS1 with the new gas-phase and aqueous-phase reactions in <b>Table 4</b> , <b>Table 5</b> , <b>Table 6</b> , and <b>Table 7</b> , together with artificial rapid conversion of MSA to sulfate for assessing the radiative effect of MSA.	1850-level
GAS_RE_2000	TS1 with the new gas-phase reactions in <b>Table 4</b> , <b>Table 5</b> , and <b>Table 6</b> , together with artificial rapid conversion of	2000-level
GAS_RE_1850	MSA to sulfate for assessing the radiative effect of MSA	1850-level

---

## 2.2 Emissions

DMS is emitted from the ocean ( $E_{\text{DMS}}$ ) via the Online Air-Sea Interface for Soluble Species (OASISS) model developed for CAM6-chem, which has been validated against observations for acetaldehyde (Wang et al., 2019b), acetone (Wang et al., 2020), and organohalogenes (e.g.  $\text{CHBr}_3$  and  $\text{CH}_2\text{Br}_2$ ) (Wang et al., 2019c). OASISS employs a two-layer framework that considers transfer velocities both through air and through water ( $k_{\text{air}}$  and  $k_{\text{water}}$ ) (Johnson, 2010):

$$E_{\text{DMS}} = k \left( [\text{DMS}]_{\text{water}} - \frac{[\text{DMS}]_{\text{air}}}{H_{\text{DMS}}} \right) (1 - f_{\text{cice}}) \quad (1)$$

$$k = \left( \frac{1}{k_{\text{water}}} + \frac{1}{k_{\text{air}}} \right)^{-1} \quad (2)$$

where  $k$  ( $\text{m s}^{-1}$ ) is the overall transfer velocity. The surface seawater concentration,  $[\text{DMS}]_{\text{water}}$  (nM) is prescribed to follow the Lana et al. (2011) sea-surface DMS climatology in both our PI and PD simulations. DMS mixing ratio in the air,  $[\text{DMS}]_{\text{air}}$ , and its Henry's Law constant, are from CAM6-chem.  $k_{\text{air}}$  is based on the NOAA COARE algorithm (Jeffery et al., 2010), which is a function of surface wind speed, with an additional adjustment for the diffusivity of still air (Mackay and Yeun, 1983).  $k_{\text{water}}$  is based on Nightingale et al. (2000), which considers sea surface temperature and salinity. Lastly,  $f_{\text{cice}}$



is the fraction of sea-ice coverage in each grid cell, such that DMS emission is suppressed from sea-ice covered surfaces.

On average, the global annual-total marine  $E_{\text{DMS}}$  is 21.5 Tg-S yr<sup>-1</sup> in [STD\_2000]. Meteorological variability has little impact on the interannual variability of emissions (<±4%). Our  $E_{\text{DMS}}$  is higher than the 18 Tg-S yr<sup>-1</sup> than the model default inventory (Kettle and Andreae, 2000), but lower than the 28 Tg-S yr<sup>-1</sup> reported in the original model study by Lana et al. (2011) and within the range of 11–28 Tg-S yr<sup>-1</sup> estimates simulated by GEOS-Chem, TOMCAT-GLOMAP and other models (Lennartz et al., 2015; Spracklen et al., 2005; Hezel et al., 2011). The estimation of  $E_{\text{DMS}}$  is sensitive to the choice of sea-surface DMS climatology; Chen et al. (2018) show that emissions vary from 18 Tg-S yr<sup>-1</sup> with the Kettle et al. (1999) DMS climatology to 22 Tg-S yr<sup>-1</sup> with the Lana et al. (2011) DMS climatology.

In all simulations, anthropogenic emissions are from the Community Emissions Data System (CEDS) (Hoesly et al., 2018) and biomass burning emissions from the CMIP6 inventory (van Marle et al., 2017). Biogenic emissions are estimated online from CLM5 using the Model of Emissions of Gases and Aerosols from Nature (MEGAN) version 2.1 (Guenther et al., 2012). CAM6-chem assumes that 2.5% by molar of sulfur emitted from the Energy & Industry sector is already in the form of primary sulfate aerosols (in accumulation mode). Volcanic emission inventories for SO<sub>2</sub> and primary sulfate are categorized by volcano types, i.e., continuously outgassing volcanos (Andres and Kasgnoc, 1998; Carn et al., 2017) and eruptive volcanoes (Mills et al., 2016). All volcanic emissions are fixed at the 2000-level in both PI and PD simulations. A breakdown of SO<sub>2</sub> emissions in this study is summarized in **Table 2**. We use the same emissions for other species as the standard CMIP6 simulations (Emmons et al., 2020).

**Table 2.** SO<sub>2</sub> emissions in this study.

Sources	Annual Total (Tg-S)	References
---------	---------------------	------------



	PI	PD	
<b>Total anthropogenic emission</b>	<b>1.14</b>	<b>54.2</b>	
Agriculture, solvents, and human waste	<0.01	0.2	(Hoesly et al., 2018)
Residential and transportation	0.4	5.2	(Hoesly et al., 2018)
Shipping	0.04	4.3	(Hoesly et al., 2018)
Energy and industry	0.7	44.4	(Hoesly et al., 2018)
Aircraft	-	0.1	(Hoesly et al., 2018)
<b>Total natural emission</b>	<b>22.9</b>	<b>22.9</b>	
Biomass burning	1.0	1.0	(van Marle et al., 2017)
Volcanos	21.9	21.9	(Andres and Kasgnoc, 1998; Carn et al., 2017; Mills et al., 2016)

### 185 2.3 Expanded DMS Oxidation Scheme

The standard CAM6-chem contains three gas-phase DMS oxidation reactions (**Table 3**) (Barth et al., 2000; Emmons et al., 2010). These reactions simplify the DMS oxidation chemistry by treating only gas-phase reactions and producing SO<sub>2</sub> directly, neglecting the role of multiphase chemistry and other key chemical products and intermediates found in chamber and field studies (e.g., Hoffmann et al., 2016; Wu et al., 2015). We note that the second reaction does not conserve sulfur.

**Table 3.** The three DMS oxidation reactions in the standard CAM6-chem.

Gas-phase Reactions	$k_{298}$ (cm <sup>3</sup> molecule <sup>-1</sup> s <sup>-1</sup> )	-E <sub>a</sub> /R (K)	References
DMS + OH → SO <sub>2</sub> (H-abstraction)	9.60 × 10 <sup>-12</sup>	-234	(Emmons et al., 2010)
DMS + OH → 0.5SO <sub>2</sub> + 0.5HO <sub>2</sub> (OH-addition)	See note <sup>a</sup>		(Emmons et al., 2010)
DMS + NO <sub>3</sub> → SO <sub>2</sub> + HNO <sub>3</sub>	1.90 × 10 <sup>-13</sup>	520	(Emmons et al., 2010)

<sup>a</sup>  $k(T, [O_2], [M]) = 1.7 \times 10^{-42} e^{(7810/T)} \times 0.21[M] / (1 + 5.5 \times 10^{-31} e^{(7460/T)} \times 0.21[M])$  (cm<sup>3</sup> molecule<sup>-1</sup> s<sup>-1</sup>)



To improve the representation of DMS oxidation in CAM6-chem, we add a suite of new reactions that describe the chemical evolution from DMS to SO<sub>2</sub>, and ultimately, sulfate via the H-abstraction and OH-addition pathways. **Figure 1** illustrates the expanded chemistry schematically. Our additions are based on recent laboratory studies and field observations and are discussed in detail in  
195 what follows.

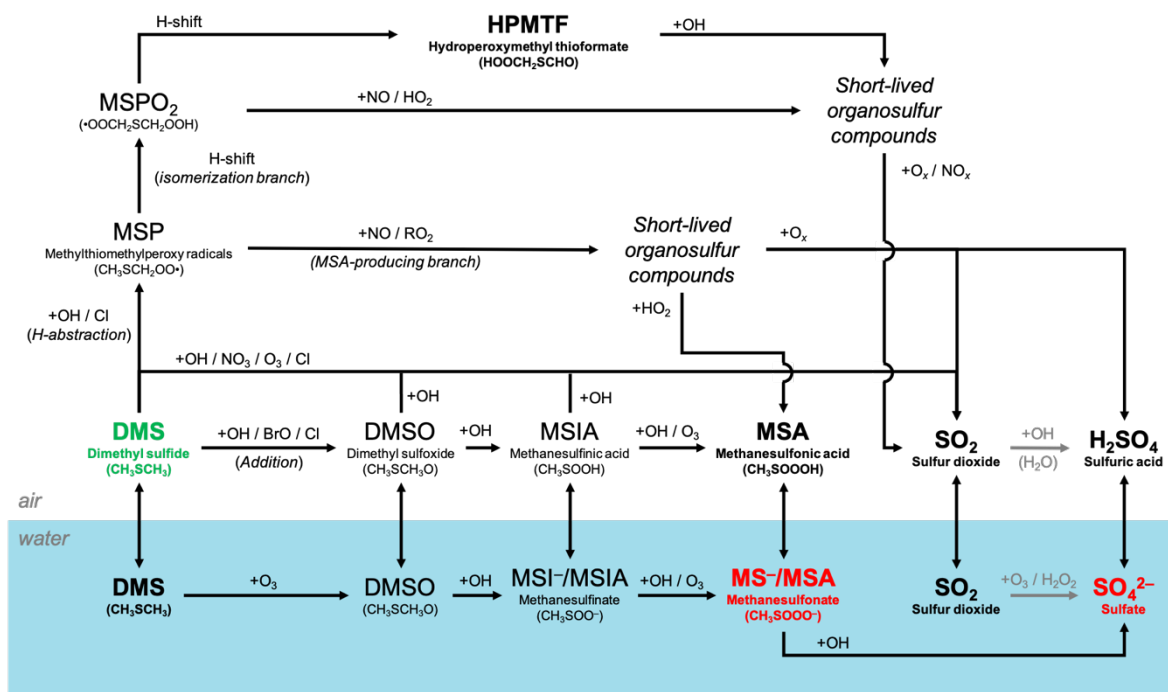


**Figure 1.** A schematic summary of our expanded chemistry of DMS oxidation in CAM6-chem (**Table 4**, **Table 5**, **Table 6**, and **Table 7**). Key relatively long-lived species (DMS, MSA, HPMTF,  $\text{SO}_2$ , and sulfate) are highlighted in bold. The blue shadings denote species and reactions in the aqueous phase in interstitial aerosols and cloud droplets. DMS (highlighted in green) can undergo O-atom addition (rightward path) or H-abstraction (upper paths). The H-abstraction channel further diverts into the isomerization branch (top path) and the MSA-producing branch.  $\text{SO}_2$  is the dominant product of most gas-phase pathways while MSA is formed mainly via the aqueous-phase oxidation of DMS. Oxidation of  $\text{SO}_2$  to sulfate or sulfuric acid is handled by the CAM6-chem standard chemistry. The resultant particulate MSA and sulfate (highlighted in red) are key species with important radiative impacts.



### 2.3.1 The H-abstraction Pathway

The H-abstraction reactions of DMS with OH or Cl generate MSP, which then either reacts with  
210 NO or RO<sub>2</sub> forming of MSA and H<sub>2</sub>SO<sub>4</sub>, or undergoes consecutive intramolecular H-shift reactions  
(isomerization), yielding HPMTF and SO<sub>2</sub>. Hence, we group these two serial reactions into two  
branches, namely the MSA-producing branch and the isomerization branch. The reactions of the MSA-  
producing branch are tabulated in **Table 4**. These reactions are largely based on Hoffmann et al. (2016),  
who combined the chemical mechanism from the Master Chemical Mechanism version 3 (MCM v3)  
215 (Saunders et al., 2003) and other laboratory and computational studies. The reactions in the  
isomerization branch are detailed in **Table 5**. Here, we use an observationally constrained isomerization  
rate of MSP ( $k_{\text{iso}}$ ) of 0.04 s<sup>-1</sup> at 293K estimated by Veres et al. (2020). This new  $k_{\text{iso}}$  is slower than the  
previously determined values of 0.23 s<sup>-1</sup> at 295K (Berndt et al., 2019) to 2.1 s<sup>-1</sup> at 293K (Wu et al.,  
2015), delaying the formation of HPMTF. A recent chamber experiment estimates an intermediate  $k_{\text{iso}}$   
220 value of 0.12 s<sup>-1</sup> at 293K (Ye et al., 2021). We investigate the impact of the uncertainty in  $k_{\text{iso}}$ , in **Sect.**  
**3**. The only chemical loss process of HPMTF in our model is oxidation by OH at a rate of  $1.11 \times 10^{-11}$   
cm<sup>3</sup> molecule<sup>-1</sup> s<sup>-1</sup> as recommended by Vermeuel et al. (2020), which is an experimentally determined  
OH-oxidation rate of MTF (a structurally similar proxy to HPMTF) by Patroescu et al. (1996).  
Oxidizing HPMTF at this rate was shown to match better with recent measurements (Vermeuel et al.,  
225 2020) than the  $1.4 \times 10^{-12}$  cm<sup>3</sup> molecule<sup>-1</sup> s<sup>-1</sup> suggested by a computational study (Wu et al., 2015).  
Recent studies (Veres et al., 2020; Vermeuel et al., 2020) suggest that cloud uptake is another important  
sink of HPMTF; we include a series of sensitivity tests based on [MOD\_2000] to address the uncertainty  
in the HPMTF budget arising from this potential loss process. Vermeuel et al. (2020) report that using  
a cloud uptake rate ( $k_{\text{HPMTF+cloud}}$ ) at  $5 \times 10^{-3}$  s<sup>-1</sup> results in a better match of diurnal variability of HPMTF  
230 with their local measurements. Due to the lack of detailed measurement, we use this  $k_{\text{HPMTF+cloud}}$  and a  
slower hypothetical value at  $5 \times 10^{-5}$  s<sup>-1</sup> for our sensitivity tests.



**Table 4.** Summary of the MSA-producing branch of the H-abstraction pathway in the DMS chemistry implemented into CAM6-chem.

Gas-phase Reactions	$k_{298}$ ( $\text{cm}^3 \text{ molecule}^{-1} \text{ s}^{-1}$ )	$-E_a/R$ (K)	References
DMS + OH $\rightarrow$ MSP (CH <sub>3</sub> SCH <sub>2</sub> OO)	$1.12 \times 10^{-11}$	-250	(Saunders et al., 2003)
DMS + Cl $\rightarrow$ 0.45MSP + 0.55(CH <sub>3</sub> ) <sub>2</sub> S(Cl) + 0.45HCl	$3.40 \times 10^{-10}$		IUPAC
(CH <sub>3</sub> ) <sub>2</sub> S(Cl) $\rightarrow$ DMS + Cl	$9.00 \times 10^1$		(Enami et al., 2004)
MSP + NO $\rightarrow$ CH <sub>3</sub> SCH <sub>2</sub> (O) + NO <sub>2</sub>	$4.90 \times 10^{-12}$	260	(Saunders et al., 2003)
MSP + RO <sub>2</sub> $\rightarrow$ CH <sub>3</sub> SCH <sub>2</sub> (O) + O <sub>2</sub>	$3.74 \times 10^{-12}$		(Saunders et al., 2003)
CH <sub>3</sub> SCH <sub>2</sub> (O) $\rightarrow$ CH <sub>3</sub> S + CH <sub>2</sub> O	$1.00 \times 10^6$		(Saunders et al., 2003)
CH <sub>3</sub> S + O <sub>3</sub> $\rightarrow$ CH <sub>3</sub> S(O) + O <sub>2</sub>	$1.15 \times 10^{-12}$	430	(Saunders et al., 2003)
CH <sub>3</sub> S + O <sub>2</sub> $\rightarrow$ CH <sub>3</sub> S(OO)	$1.20 \times 10^{-16}$	1580	(Saunders et al., 2003)
CH <sub>3</sub> S(O) + O <sub>3</sub> $\rightarrow$ CH <sub>3</sub> (O <sub>2</sub> ) + SO <sub>2</sub>	$4.00 \times 10^{-13}$		(Saunders et al., 2003)
CH <sub>3</sub> S(OO) $\rightarrow$ CH <sub>3</sub> (O <sub>2</sub> ) + SO <sub>2</sub>	$5.60 \times 10^{16}$	-10870	(Saunders et al., 2003)
CH <sub>3</sub> S(OO) $\rightarrow$ CH <sub>3</sub> SO <sub>2</sub>	1.00		(Saunders et al., 2003)
CH <sub>3</sub> SO <sub>2</sub> + O <sub>3</sub> $\rightarrow$ CH <sub>3</sub> SO <sub>3</sub> + O <sub>2</sub>	$3.00 \times 10^{-13}$		(Saunders et al., 2003)
CH <sub>3</sub> SO <sub>2</sub> $\rightarrow$ CH <sub>3</sub> (O <sub>2</sub> ) + SO <sub>2</sub>	$5.00 \times 10^{13}$	-9673	(Saunders et al., 2003)
CH <sub>3</sub> SO <sub>3</sub> + HO <sub>2</sub> $\rightarrow$ MSA + O <sub>2</sub>	$5.00 \times 10^{-11}$		(Saunders et al., 2003)
CH <sub>3</sub> SO <sub>3</sub> $\rightarrow$ CH <sub>3</sub> (O <sub>2</sub> ) + H <sub>2</sub> SO <sub>4</sub>	$5.00 \times 10^{13}$	-9946	(Saunders et al., 2003)

**Table 5.** Summary of the isomerization branch of the H-abstraction pathway in the DMS chemistry implemented into CAM6-chem.

Gas-phase Reactions	$k_{298}$ ( $\text{cm}^3 \text{ molecule}^{-1} \text{ s}^{-1}$ )	$-E_a/R$ (K)	References
MSP $\rightarrow$ OOC <sub>2</sub> H <sub>4</sub> SCH <sub>2</sub> OOH	See note <sup>a</sup>		(Veres et al., 2020)
OOC <sub>2</sub> H <sub>4</sub> SCH <sub>2</sub> OOH $\rightarrow$ HPMTF (HOOCH <sub>2</sub> SCHO) + OH	See note <sup>b</sup>		(Veres et al., 2020)
OOC <sub>2</sub> H <sub>4</sub> SCH <sub>2</sub> OOH + NO $\rightarrow$ HOOCH <sub>2</sub> SCH <sub>2</sub> O + NO <sub>2</sub>	$4.90 \times 10^{-12}$	260	(Saunders et al., 2003)



$\text{HOCH}_2\text{SCH}_2\text{O} \rightarrow \text{HOCH}_2\text{S} + \text{CH}_2\text{O}$	$1.00 \times 10^6$		(Saunders et al., 2003)
$\text{OOCH}_2\text{SCH}_2\text{OOH} + \text{HO}_2 \rightarrow \text{HOCH}_2\text{SCH}_2\text{OOH} + \text{O}_2$	$1.13 \times 10^{-13}$	1300	(Saunders et al., 2003)
$\text{HPMTF} + \text{OH} \rightarrow \text{HOCH}_2\text{SCO} + \text{H}_2\text{O}$	$1.11 \times 10^{-11}$		(Patroescu et al., 1996; Vermeuel et al., 2020)
$\text{HOCH}_2\text{SCO} \rightarrow \text{HOCH}_2\text{S} + \text{CO}$	$9.20 \times 10^9$	-505.4	(Wu et al., 2015)
$\text{HOCH}_2\text{SCO} \rightarrow \text{OH} + \text{CH}_2\text{O} + \text{OCS}$	$1.60 \times 10^7$	-1468.6	(Wu et al., 2015)
$\text{HOCH}_2\text{S} + \text{O}_3 \rightarrow \text{HOCH}_2\text{SO} + \text{O}_2$	$1.15 \times 10^{-12}$	430	(Saunders et al., 2003)
$\text{HOCH}_2\text{S} + \text{NO}_2 \rightarrow \text{HOCH}_2\text{SO} + \text{NO}$	$6.00 \times 10^{-11}$	240	(Saunders et al., 2003)
$\text{HOCH}_2\text{SO} + \text{O}_3 \rightarrow \text{SO}_2 + \text{CH}_2\text{O} + \text{OH} + \text{O}_2$	$4.00 \times 10^{-13}$		(Saunders et al., 2003)
$\text{HOCH}_2\text{SO} + \text{NO}_2 \rightarrow \text{SO}_2 + \text{CH}_2\text{O} + \text{OH} + \text{NO}$	$1.20 \times 10^{-11}$		(Saunders et al., 2003)

<sup>a</sup>  $2.24 \times 10^{11} \exp(-9.8 \times 10^3 / T) \exp(1.03 \times 10^8 / T^3)$

<sup>b</sup>  $6.09 \times 10^{11} \exp(-9.5 \times 10^3 / T) \exp(1.1 \times 10^8 / T^3)$

where  $T$  is air temperature.

### 235 2.3.2 Gas-phase reactions of the OH-addition Pathway

**Table 6** summarizes the new gas-phase reactions in the OH-addition pathway of DMS oxidation. We update the gas-phase reactions in the model to consider the oxidation of DMS by not only OH and NO<sub>3</sub> but also BrO, O<sub>3</sub>, and Cl as recommended or reported in previous studies, e.g., Barnes et al. (2006), Hoffmann et al. (2016), and Chen et al. (2018). The new reactions producing dimethyl sulfoxide (DMSO: CH<sub>3</sub>SCH<sub>3</sub>O), methanesulfinic acid (MSIA: CH<sub>3</sub>SOOH), and MSA intermediates, are added to the model as new advected chemical tracers which undergo not only chemical production and loss but also transport and deposition. MSA and SO<sub>2</sub> are terminating products of these new gas-phase OH-addition pathway reactions, which is consistent with various modeling studies, e.g., Pham et al. (1995), Spracklen et al. (2005), and Chen et al. (2018). All oxidants (OH, O<sub>3</sub>, H<sub>2</sub>O<sub>2</sub>, BrO, and HOBr) are simulated online by the standard gas-phase chemistry scheme of CAM6-chem.



**Table 6.** Gas-phase DMS oxidation (OH-addition pathway) implemented into CAM6-chem in this study.

Gas-phase Reactions	$k_{298}$ ( $\text{cm}^3 \text{ molecule}^{-1} \text{ s}^{-1}$ )	$-E_a/R$ (K)	References
$\text{DMS} + \text{OH} \rightarrow 0.6\text{SO}_2 + 0.4\text{DMSO} + \text{CH}_3\text{O}_2$	See note <sup>a</sup>	-	(Burkholder et al., 2015; Pham et al., 1995)
$\text{DMS} + \text{NO}_3 \rightarrow$ $\text{SO}_2 + \text{HNO}_3 + \text{CH}_3\text{O}_2 + \text{CH}_2\text{O}$	$1.13 \times 10^{-12}$	530	(Burkholder et al., 2015)
$\text{DMS} + \text{BrO} \rightarrow \text{DMSO} + \text{Br}$	$3.39 \times 10^{-13}$	950	(Burkholder et al., 2015)
$\text{DMS} + \text{O}_3 \rightarrow \text{SO}_2$	$1.00 \times 10^{-19}$	0	(Burkholder et al., 2015)
$\text{DMS} + \text{Cl} \rightarrow$ $0.5\text{SO}_2 + 0.5\text{DMSO} + 0.5\text{HCl} + 0.5\text{ClO}$	$3.40 \times 10^{-10}$	0	(Burkholder et al., 2015)
$\text{DMSO} + \text{OH} \rightarrow 0.95\text{MSIA} + 0.05\text{SO}_2$	$8.94 \times 10^{-11}$	800	(Burkholder et al., 2015)
$\text{MSIA} + \text{OH} \rightarrow 0.9\text{SO}_2 + 0.1\text{MSA}$	$9.00 \times 10^{-11}$	0	(Burkholder et al., 2015)
$\text{MSIA} + \text{O}_3 \rightarrow \text{MSA}$	$2.00 \times 10^{-18}$	0	(Lucas, 2002)

$$^a k(T, [\text{O}_2], [\text{M}]) = 8.2 \times 10^{-39} [\text{O}_2] e^{(5376/T)} / (1 + 1.05 \times 10^{-5} ([\text{O}_2]/[\text{M}]) e^{(3644/T)}) \text{ (cm}^3 \text{ molecule}^{-1} \text{ s}^{-1})$$

### 2.3.3 Aqueous-phase reactions of the OH-addition Pathway

We also introduce new aqueous-phase reactions of the OH-addition pathway as shown in **Table 7**.

**Table 7.** Aqueous-phase DMS oxidation (OH-addition pathway) implemented into CAM6-chem in this study.

Aqueous-phase Reactions	$k_{298}$ ( $\text{M}^{-1} \text{ s}^{-1}$ )	$-E_a/R$ (K)	References
$\text{DMS}_{(\text{aq})} + \text{O}_3_{(\text{aq})} \rightarrow \text{DMSO}_{(\text{aq})} + \text{O}_2_{(\text{aq})}$	$8.61 \times 10^8$	-2600	(Gershenson et al., 2001)
$\text{DMSO}_{(\text{aq})} + \text{OH}_{(\text{aq})} \rightarrow \text{MSIA}_{(\text{aq})}$	$6.63 \times 10^9$	-1270	(Zhu et al., 2003)



$\text{MSIA}_{(\text{aq})} + \text{OH}_{(\text{aq})} \rightarrow \text{MSA}_{(\text{aq})}$	$6.00 \times 10^9$	0	(Sehested and Holcman, 1996)
$\text{MSI}^{-}_{(\text{aq})} + \text{OH}_{(\text{aq})} \rightarrow \text{MSA}_{(\text{aq})}$	$1.20 \times 10^{10}$	0	(Bardouki et al., 2003)
$\text{MSIA}_{(\text{aq})} + \text{O}_3_{(\text{aq})} \rightarrow \text{MSA}_{(\text{aq})}$	$3.50 \times 10^7$	0	(Hoffmann et al., 2016)
$\text{MSI}^{-}_{(\text{aq})} + \text{O}_3_{(\text{aq})} \rightarrow \text{MSA}_{(\text{aq})}$	$2.00 \times 10^6$	0	(Flyunt et al., 2001)
$\text{MSA}_{(\text{aq})} + \text{OH}_{(\text{aq})} \rightarrow \text{SO}_4^{2-}_{(\text{aq})}$	$1.50 \times 10^7$	0	(Hoffmann et al., 2016)
$\text{MS}^{-}_{(\text{aq})} + \text{OH}_{(\text{aq})} \rightarrow \text{SO}_4^{2-}_{(\text{aq})}$	$1.29 \times 10^7$	-2630	(Zhu et al., 2003)

Following a similar treatment employed by the Community Multiscale Air Quality (CMAQ) Model version 5.1 (Fahey et al., 2017), we calculate, for each species involved in the new aqueous-  
 255 phase reactions, the phase transfer equations for gas-aqueous partitioning as below:

$$\frac{dC_g}{dt} = -k_{(\text{g}) \rightarrow (\text{a})} C_g + k_{(\text{a}) \rightarrow (\text{g})} C_a = -(k_t \text{LWC}) C_g + \left(\frac{k_t}{HRT}\right) C_a \quad (3)$$

$$\frac{dC_a}{dt} = k_{(\text{g}) \rightarrow (\text{a})} C_g - k_{(\text{a}) \rightarrow (\text{g})} C_a = (k_t \text{LWC}) C_g - \left(\frac{k_t}{HRT}\right) C_a \quad (4)$$

$$k_t = \left(\frac{r^2}{3D_g} + \frac{4r}{3c\alpha}\right)^{-1} \quad (5)$$

where  $C_g$  and  $C_a$  are the gas-phase and aqueous-phase concentration of a species involving in reactions  
 260 in **Table 7**;  $k_{(\text{g}) \rightarrow (\text{a})}$ ,  $k_{(\text{a}) \rightarrow (\text{g})}$  ( $\text{s}^{-1}$ ) are its gas-to-aqueous and aqueous-to-gas phase-transfer coefficients;  $k_t$  ( $\text{s}^{-1}$ ) is its base phase-transfer coefficient;  $H$  ( $\text{M atm}^{-1}$ ) is its effective Henry's Law constant;  $r$  (cm) is its mean particle radius;  $D_g$  is gas phase diffusion coefficient (assumed at  $0.1 \text{ cm}^2 \text{ s}^{-1}$  here following Dentener and Crutzen (1993));  $c$  ( $\text{cm s}^{-1}$ ) is its thermal speed, and;  $\alpha$  is its mass accommodation coefficient. Values of  $H$  and  $\alpha$  for DMS, DMSO, MSIA, and MSA are given in **Table 8**. LWC ( $\text{cm}^3$ -  
 265 water ( $\text{cm}^3\text{-air}^{-1}$ ) is liquid water content of interstitial aerosol determined by MOSAIC (Zaveri et al., 2021) or cloud liquid water content calculated by the CAM6;  $R=0.082$  ( $\text{L atm K}^{-1} \text{ mol}^{-1}$ ) is the universal gas constant, and;  $T$  (K) is air temperature.



**Table 8.** Summary of parameters of DMS and its oxidation intermediates used in this study.

	$H_{298}$ (Henry's Law Coefficients at 298K) [M/atm] <sup>a, b</sup>	$-E/R$ (Heat of dissolution for H298)/R [K] <sup>a, b</sup>	$K_1$ (acid dissociation constant) [M] <sup>b</sup>	$\alpha$ (mass accommodation coefficient) <sup>c</sup>	molar mass [g/mol] <sup>a</sup>
DMS	0.54	3460	-	0.001	62.1324
DMSO	10 <sup>7</sup>	2580	-	0.1	78.13
MSIA	10 <sup>8</sup>	1760	-2.28	0.1	80.11
MSA	10 <sup>9</sup>	1760	1.86	0.1	96.1

Reference:

<sup>a</sup> Lamarque et al. (2012)

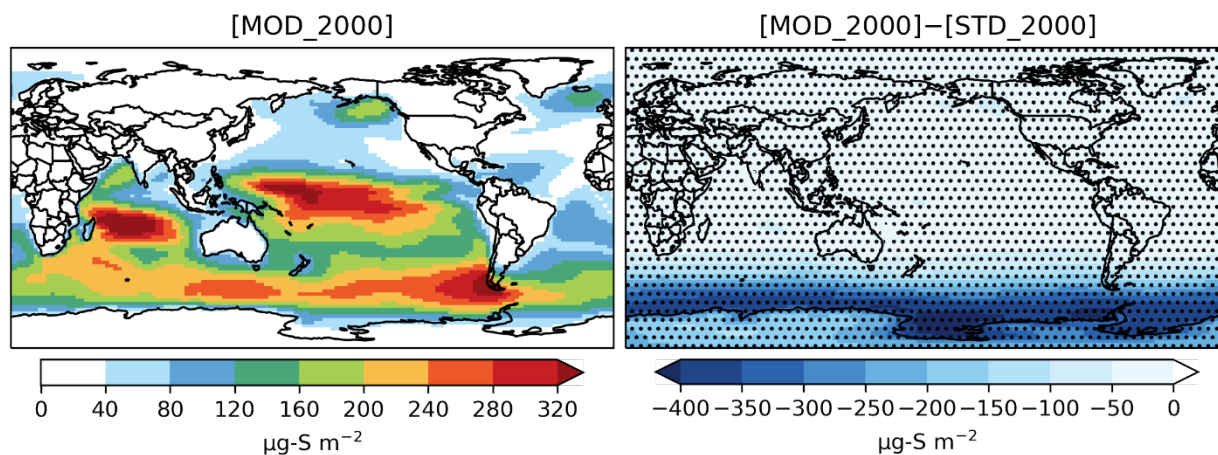
<sup>b</sup> Chen et al. (2018)

<sup>c</sup> Zhu et al. (2006)

## 270 3 Implications of the Extended DMS Oxidation Mechanism

### 3.1 Global sulfur budget and distribution in present-day

The global burden of DMS in [MOD\_2000] is 50 Gg-S. It is 38% lower than the standard run, [STD\_2000], but remains within the range of 9.6–140 Gg-S from other studies (Faloona, 2009; Kloster et al., 2006). **Figure 2** shows the reduction is mainly over the Southern Ocean and is attributable to  
275 faster chemical losses via DMS+BrO and DMS<sub>(aq)</sub>+O<sub>3(aq)</sub> (**Figure 3**). The global lifetime of DMS decreases from 1.5 days in [STD\_2000] to 0.8 days in [MOD\_2000]. These values are comparable to the range of 1.2–2.1 days reported in Chen et al., (2018).



280 **Figure 2.** Spatial distribution of annual-mean column concentration ( $\mu\text{g-S m}^{-2}$ ) for DMS simulated by [MOD\_2000] (left), and its difference from the baseline run, i.e. [MOD\_2000]-[STD\_2000] (right). Dotted regions (nearly worldwide) indicate where statistically significant differences are identified by grid-by-grid two-sample t-tests with  $p$ -values  $< 0.05$ .

285 Globally, chemical loss is the largest sink of DMS ( $\sim 24 \text{ Tg-S yr}^{-1}$ ) in both PD simulations. The model default chemistry in [STD\_2000] predicts that OH oxidation makes up 40% (H-abstraction) and 39% (OH-addition) of DMS chemical removal globally while the remaining portion is attributed to  $\text{NO}_3$  oxidation. These three reactions are only responsible for 80% of global DMS loss in [MOD\_2000]. **Figure 3** shows that, in [MOD\_2000], DMS is mainly oxidized by OH in the gas phase (34% via the

290 H-abstraction channel and 23% via the OH-addition pathway) which contributes up to 80% of local loss over the tropical oceans, where surface OH is the highest. The annual-mean surface concentrations of all oxidants which react with DMS in our updated scheme are summarized in **Figure S1**.  $\text{NO}_3$  oxidation of DMS accounts for 23% of global DMS chemical loss and is dominant in Northern Hemisphere mid-latitudes, where the outflow of nitrogen oxides ( $\text{NO}_x$ ) – precursors of atmospheric

295  $\text{NO}_3$  – from land are substantial (Miyazaki et al., 2012). DMS oxidation by  $\text{NO}_3$  contributes  $< 10\%$  over most marine environments in the Southern Hemisphere. Previous studies estimate that the global



contribution of OH and NO<sub>3</sub> to DMS oxidation range ~50–70% and 15–30%, respectively (Berglen, 2004; Boucher et al., 2003; Khan et al., 2016; Chen et al., 2018).

Oxidation by BrO is responsible for 11% of global DMS removal, which falls midway within  
300 the previously estimated range of 8–29% (Boucher et al., 2003; Khan et al., 2016; Chen et al., 2018). Regionally, its importance can be up to 50–60% over the high latitudes in the Southern Hemisphere, which is close to a previous box model experiment (Hoffmann et al., 2016).

DMS+O<sub>3</sub> is the only multi-phase DMS oxidation reaction in this study, accounting for 8%  
(aqueous-phase) and 0.4% (gas-phase) of global DMS depletion. The oxidation rates via these reactions  
305 estimated by Boucher et al. (2003) were 6% and 3% of the total DMS sink calculated, respectively. Our lower gas-phase DMS+O<sub>3</sub> reaction rate could be due to the inclusion of the BrO oxidation, which is missing in their study. Regionally, the fractional contribution of aqueous-phase DMS+O<sub>3</sub> to DMS oxidation can be up to 20–30% over high-latitude oceans, which is on the upper end of the range of 5–30% high-latitude DMS losses previously reported (von Glasow and Crutzen, 2004; Chen et al., 2018).

310 Lastly, the Cl oxidation reactions via either the addition or abstraction channels contribute equally (0.3% each, globally) to the chemical removal of DMS, which is consistent with the proposal of (Atkinson et al., 2004). Our estimated values are much lower than the 4% found in a global model study (Chen et al., 2018) and the 8–18% from box-model studies (von Glasow and Crutzen, 2004; Hoffmann et al., 2016).

315

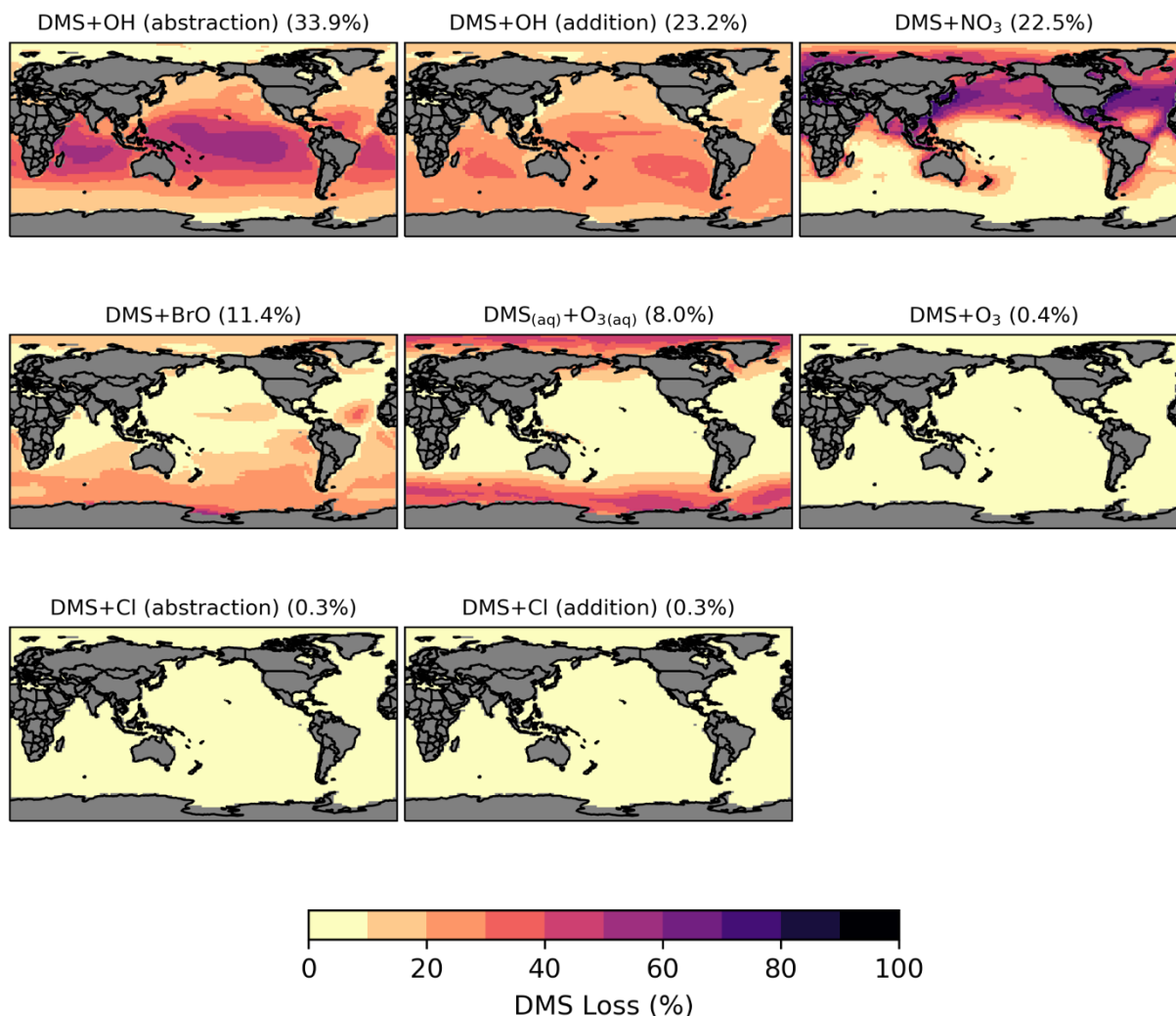
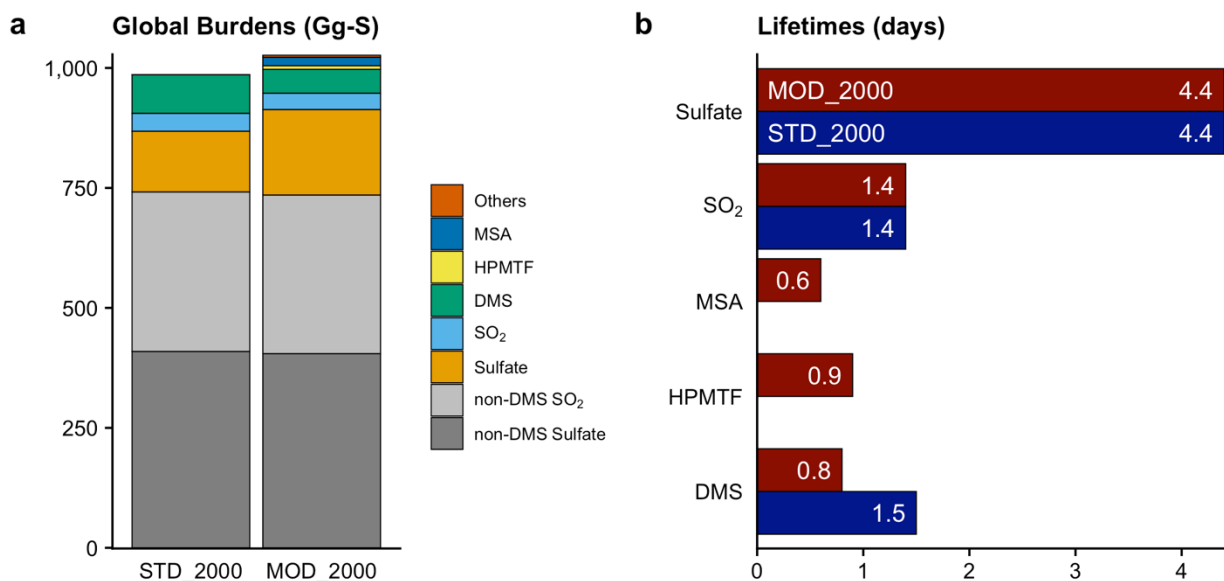


**Figure 3.** Spatial distribution of fractional DMS oxidation (%) from [MOD\_2000] through DMS+OH (abstraction), DMS+OH (addition), DMS+NO<sub>3</sub>, DMS+BrO, DMS<sub>(aq)</sub>+O<sub>3(aq)</sub>, DMS+O<sub>3</sub>, DMS+Cl (abstraction), and DMS+Cl (addition). Percentages in the brackets denote contribution to global chemical loss. Subplots are arranged in descending order of their annual-total oxidation rates.



The global atmospheric sulfur burden is increased by 41 Gg-S (or 4.1%) from [STD\_2000] to [MOD\_2000] (**Figure 4** and **Table S1**). Approximately half (23 Gg-S) of this increment is associated with the recovery of the missing sulfur associated with the OH-addition reaction in the standard chemistry (the second reaction in **Table 3**), which does not conserve sulfur. The remaining total sulfur burden increase is attributable to the extended chemistry scheme. As discussed above, the DMS burden in [MOD\_2000] is lower than [STD\_2000] by 38% due to faster oxidation. This oxidation produces intermediates with a wide range of lifetimes. The addition of intermediates with relatively long physical lifetimes (to dry and wet deposition only) of HPMTF (1,300 days) and MSA (8.5 days) delays the formation of SO<sub>2</sub> (2.6 days) and sulfate (4.4 days) compared to the standard reactions in [STD\_2000], which increases the export of sulfur-containing intermediates.





335 **Figure 4. (a)** Global burdens of various atmospheric sulfur species in our simulations. “Others” includes all other sulfur-containing intermediates in the new chemistry, e.g., DMSO, MSIA, etc. SO<sub>2</sub> (blue) and sulfate (orange) refer to the burden of these species that originate from DMS oxidation only; non-DMS contributions are shown in grey. **(b)** Total lifetimes of the atmospheric sulfur species to both physical and chemical losses.

340

The PD global annual mean burden for sulfate aerosol is 582 Gg-S in [MOD\_2000], with an interannual variability of 46 Gg-S (standard deviation of annual means). It is comparable to the 580 Gg-S in a previous CAM6-chem study (Tilmes et al., 2019) and is within the estimates (420–660 Gg-S) from studies using other models (Heald et al., 2014; Chen et al., 2018). The new DMS chemistry has  
345 increased the global sulfate burden by 47 Gg-S (or 8.8%) from the baseline value of 535 Gg-S in [STD\_2000]. The statistically significant increases in sulfate resulting from the expanded chemistry are mostly found over the tropical and sub-tropical oceans in the Southern Hemisphere (**Figure 5**). There is no strong seasonality in the additional sulfate produced from our expanded chemistry. We estimate that the sulfate burden attributable to DMS increases by 41% from 126 Gg-S in [STD\_2000] to 178  
350 Gg-S in [MOD\_2000]. Most of this increase in sulfate burden (72%) comes from the expansion of the gas-phase chemistry with a minor additional contribution from the aqueous-phase chemistry. In a sensitivity test where the isomerization branch reaction (**Table 5**) is removed from [MOD\_2000], the global DMS-derived sulfate burden is reduced by 2.0% (relative to [MOD\_2000]).



355

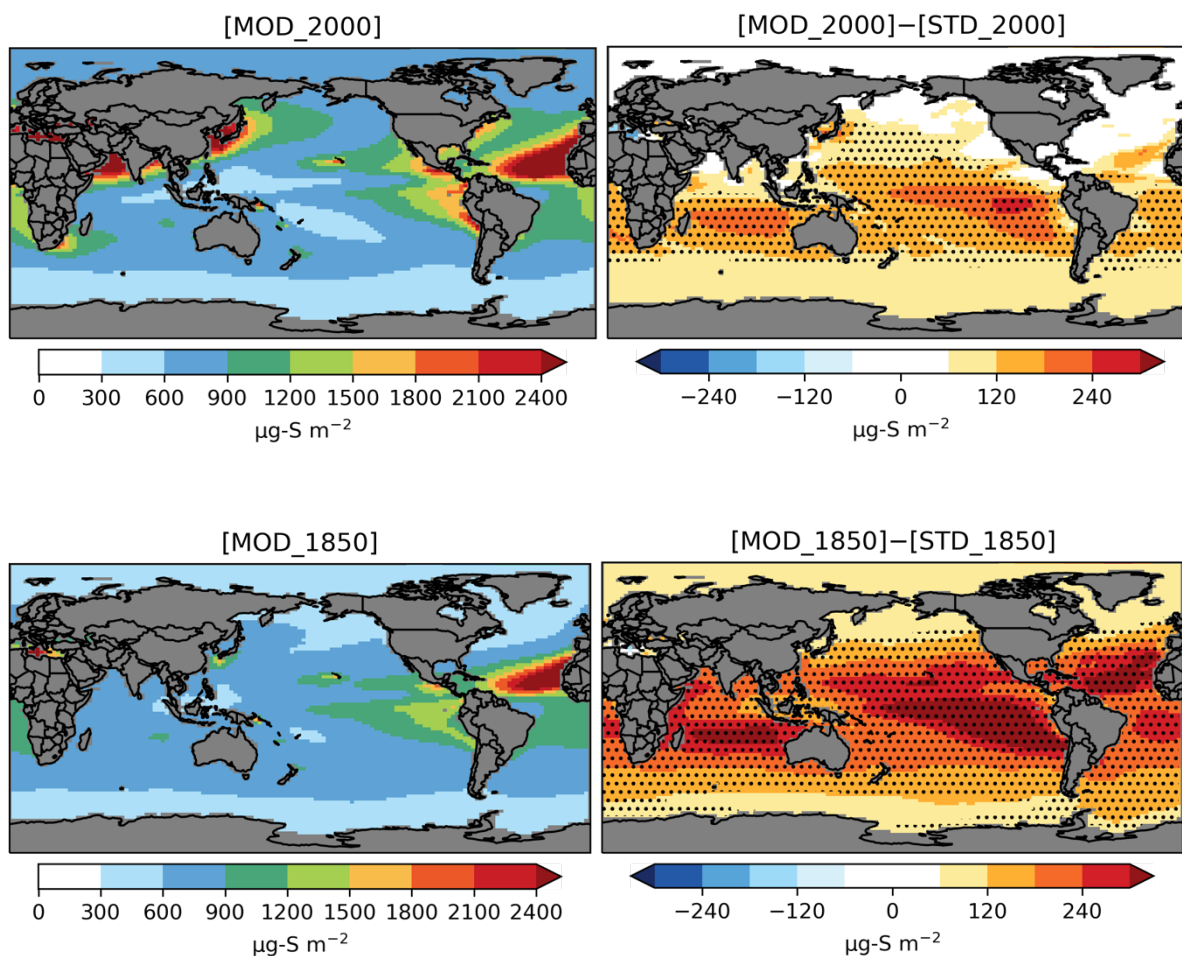
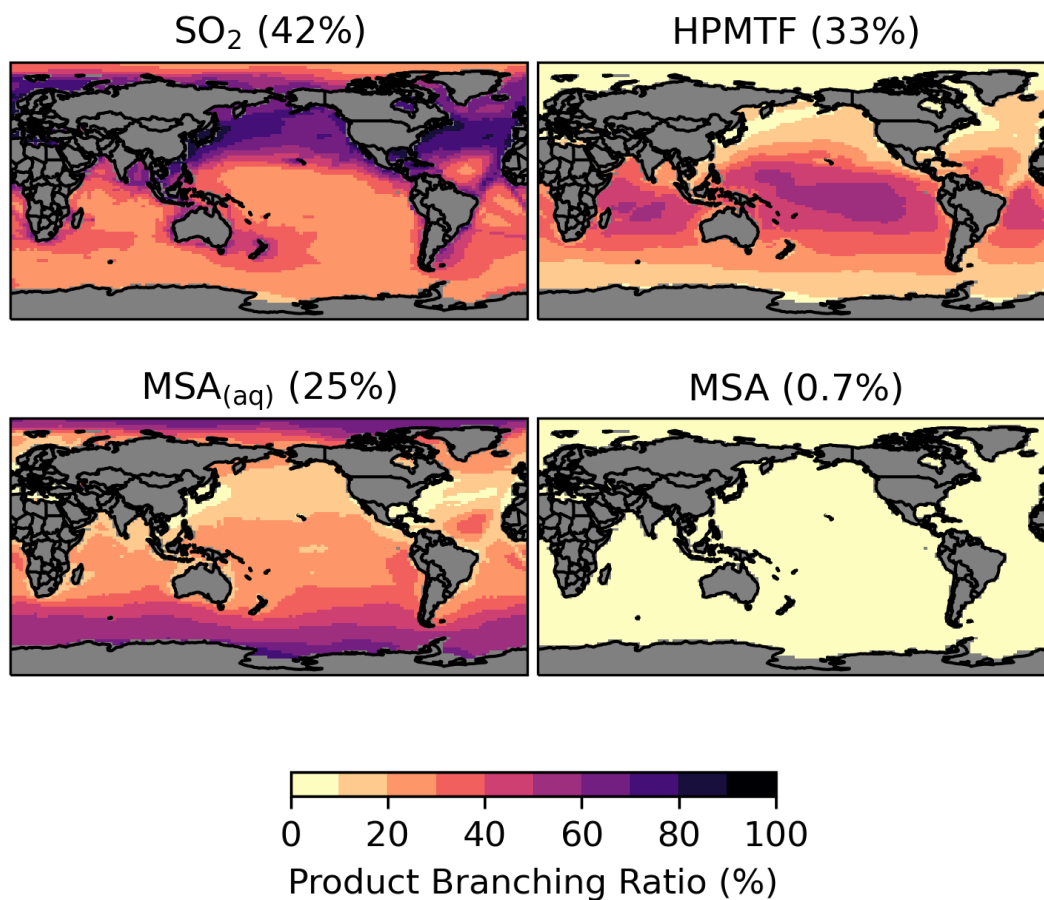


**Figure 5.** Spatial distribution of annual-mean column concentrations ( $\mu\text{g-S m}^{-2}$ ) for sulfate aerosol simulated by [MOD] (left column), and their difference from the baseline run (right column). Only values over the ocean are shown. Dotted regions indicate where statistically significant differences are identified by grid-by-grid two-sample t-tests with  $p$ -values  $< 0.05$ .



The spatial distribution of the product branching ratios of DMS oxidation is shown in **Figure 6**. In addition to depositional removal, HPMTF converts into SO<sub>2</sub> while SO<sub>2</sub> and MSA are then oxidized to form sulfate. We estimate that 33% of the annual-total DMS oxidation will yield HPMTF. This is comparable to the observationally constrained estimates from ATom-3 and ATom-4 flight campaigns, that ~30–40% DMS was oxidized to HPMTF along their flight tracks (Veres et al., 2020). High HPMTF production is typically seen in the summer MBL, coinciding with the HPMTF hotspots over tropical oceans as shown in **Figure S2**. To address the uncertainty in the production and loss of HPMTF as discussed in **Sect. 2.3**, we run several sensitivity tests using five combinations of  $k_{\text{iso}}$  and  $k_{\text{HPMTF+cloud}}$  values based on [MOD\_2000]. **Table S2** and **Figure S5** summarize the key results of these sensitivity tests. Compared to [MOD\_2000], we find that using a faster  $k_{\text{iso}}$  of 0.12 s<sup>-1</sup> at 293 K (Ye et al., 2021) increases the global annual-total isomerization rate of MSP by 5.6% while the global burden of HPMTF increases by 4.1%. Increasing the isomerization rate has little impact on the burden of sulfate from DMS (increase of only 4.0%). We also evaluate the importance of cloud uptake of HPMTF with two hypothetical values of  $k_{\text{HPMTF+cloud}}$  at  $5 \times 10^{-3}$  s<sup>-1</sup> (Vermeuel et al., 2020) and  $5 \times 10^{-5}$  s<sup>-1</sup>. At these rates, cloud uptake becomes an important sink of HPMTF, responsible for 68–69% and 28% of total HPMTF losses respectively. The corresponding global burdens of HPMTF are substantially lowered by 85–86% and 52%. For simulation with cloud uptake loss, the burdens of HPMTF and sulfate are much less sensitive to our choice of  $k_{\text{iso}}$  due to the rapid loss of HPMTF to cloud uptake. In these sensitivity simulations, the sulfur contained in HPTMF is assumed to be removed from the system once taken up by cloud, thus reducing the sequential formation of SO<sub>2</sub> and sulfate (by up to 8 %).



385

**Figure 6.** Branching ratio (%) of the multi-phase DMS oxidation pathways in [MOD\_2000], considering HPMTF,  $\text{SO}_2$ , and MSA as terminating products estimated from their annual-total production rates.

390 MSA is a key intermediate generated from the OH-addition channel of the multi-phase DMS oxidation, especially, over remote marine atmosphere. Our result shows that aqueous-phase MSA formation accounts for most of MSA production as commonly reported (von Glasow and Crutzen, 2004; Barnes et al., 2006; Zhu et al., 2006; Hoffmann et al., 2016; Chen et al., 2018). In [MOD\_2000], the global MSA burden is 7.5 Gg-S, which is smaller than the range of 13–40 Gg-S from previous model



395 studies (Pham et al., 1995; Chin et al., 1996, 2000; Cosme et al., 2002; Hezel et al., 2011; Chen et al.,  
2018). In [MOD\_2000]. Most MSA is formed over the Southern Ocean (**Figure S3**). The lifetime of  
MSA is 0.6 days globally, shorter than the 5–7 days previously proposed (Chin et al., 1996, 2000;  
Cosme et al., 2002; Hezel et al., 2011; Pham et al., 1995), likely because we include the aqueous-phase  
OH-oxidation to sulfate which is a significant loss process for MSA. This oxidation accounts for ~76%  
400 of removal in [MOD\_2000], followed by cloud uptake (18%).

### 3.2 Comparison with observations

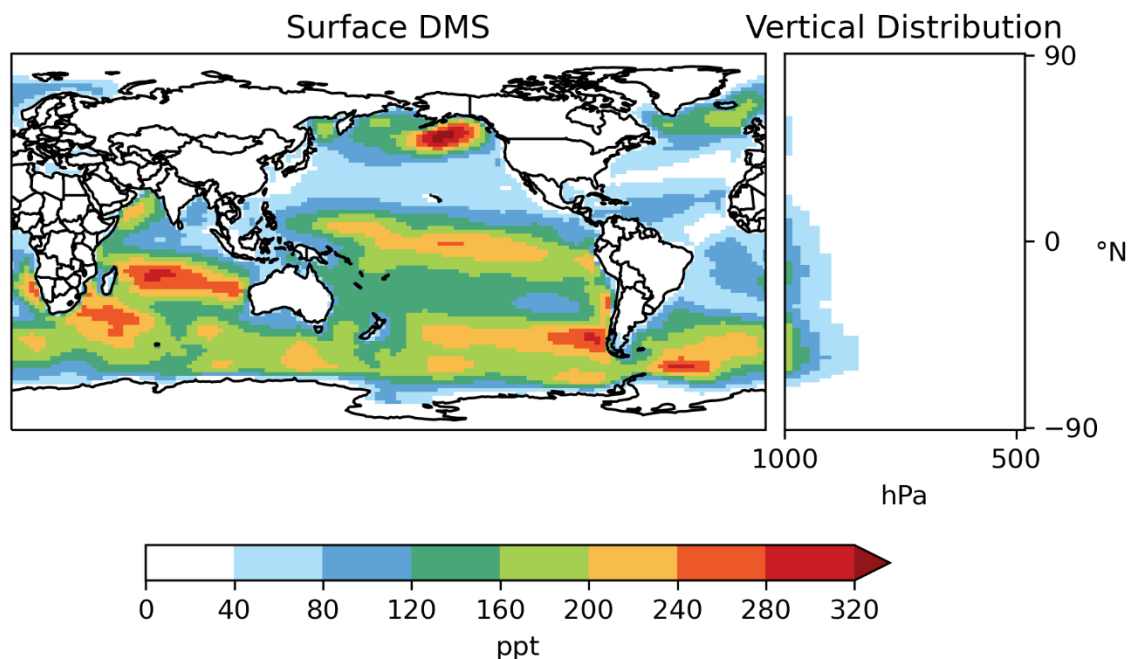
**Table 9** summarizes the key observational datasets used here to compare with our PD model  
simulations for their wide coverage of the remote marine atmosphere. The VAMOS Ocean-Cloud-  
405 Atmosphere-Land Study Regional Experiment (VOCALS-REx) is an international field project that  
took place during October and November in 2008 over southeastern Pacific off northern Chile and  
southern Peru (Wood et al., 2011). VOCAL-REx consists of both ship-based and airborne  
measurements for lower-atmospheric DMS,  $\text{MSA}_{(\text{aq})}$ , and non-sea-salt sulfate aerosol ( $\text{nss-SO}_4^{2-}{}_{(\text{aq})}$ ).  
The Atmospheric Tomography (ATom) mission of NASA is a flight campaign spanning from the Arctic  
410 to the Antarctic over the remote Pacific and Atlantic Oceans between 2016 and 2018, (Wofsy et al.,  
2018). During ATom, an array of instruments was used to collect and analyze daytime air samples from  
the remote marine environments, providing measurements of DMS, HPMTF,  $\text{MSA}_{(\text{aq})}$ , and  $\text{nss-SO}_4^{2-}{}_{(\text{aq})}$ .  
The Aerosol and Cloud Experiments in the Eastern North Atlantic (ACE-ENA) probed the  
atmosphere surrounding the ENA observatory on Graciosa Island during summer 2017 and winter 2018  
415 (Wang et al., 2019a, 2021). ACE-ENA provides high time-resolution in-situ measurements of MSA  
and sulfate aerosol in the lower troposphere (Zawadowicz et al., 2021). We note that the model-  
measurement comparisons are not exact, given that our simulations are performed using free-running  
dynamics and thus are not paired to the meteorological year of measurements. We therefore sample  
monthly mean values from the model at the location of the observations to provide qualitative  
420 comparisons.



**Table 9.** Key observational datasets used in this study.

Mission	Aliases	Instruments	Species Measured	Reference
VOCALS-REx	OBS_BROWN	Quadrupole mass spectrometry on Research Vessel (R/V) Ronald H. Brown	DMS	(Huebert et al., 2004)
	OBS_C130	Quadrupole mass spectrometry on NSF/NCAR Lockheed C-130 aircraft	DMS	(Booth and Powell, 2006)
ATom	OBS_PILS	Particle into liquid sampler (PILS) on Department of Energy (DoE) Gulfstream-1 (G-1) aircraft	MSA <sub>(aq)</sub> , nss-SO <sub>4</sub> <sup>2-</sup> <sub>(aq)</sub>	(Allen et al., 2011)
	OBS_AMS	Aerosol mass spectrometry (AMS) and two-stage impactor (TSI) on R/V Ronald H. Brown	MSA <sub>(aq)</sub> , nss-SO <sub>4</sub> <sup>2-</sup> <sub>(aq)</sub>	(Huebert et al., 2004)
	OBS_WAS	Whole Air Sampling (WAS)	DMS	(Simpson et al., 2001)
	OBS_TOGA	Trace Organic Gas Analyzer (TOGA)	DMS	(Apel et al., 2015)
	OBS_CIMS	Iodide-ion chemical ionization time-of-flight mass spectrometer (CIMS)	HPMTF	(Veres et al., 2020)
ACE-ENA	OBS_AMS	high-resolution time-of-flight mass spectrometer (HR-ToF-AMS)	MSA <sub>(aq)</sub> , nss-SO <sub>4</sub> <sup>2-</sup> <sub>(aq)</sub>	(Canagaratna et al., 2007)
	OBS_AMS	HR-ToF-AMS	MSA <sub>(aq)</sub> , nss-SO <sub>4</sub> <sup>2-</sup> <sub>(aq)</sub>	(Zawadowicz et al., 2021)

Most DMS resides in the lower troposphere (**Figure 7**). Annual-mean surface DMS from [MOD\_2000] ranges from 40-300 ppt over much of the ocean, but can exceed 320 ppt over the Southern Ocean and northeastern Pacific, regions with high DMS emissions. DMS concentrations of ~25–125 ppt were observed at Cape Grim, Australia in 1990-1993 (Ayers et al., 1995). Sciare et al. (2000) report an annual-mean DMS of 181 ppt at Amsterdam Island in the Indian Ocean during the 1990s. Both values are in line with the surface DMS at the corresponding locations modeled by [MOD\_2000].



430

**Figure 7.** Horizontal distribution of annual-mean surface mixing ratio and zonal-mean vertical distribution of DMS (both in ppt) modeled by [MOD\_2000].

**Figure 8** summarizes the spatial difference between the observed DMS from the VOCALS-  
435 REx and ATom missions and the simulated DMS. The model captures the peaks over the tropical Pacific and the Southern Oceans off the coast of South America, but aircraft measurements detect hotspots that are not simulated by the model (**Figure 8(a)**). During VOCALS-REx the ship-based measurements (BROWN) recorded a range of near-surface DMS from 18 ppt to 111 ppt, while the airborne measurements (C130) reveal a vertically decreasing trend of DMS mixing ratios, from 33 ppt  
440 at ~500 m to 2.0 ppt at ~2 km (**Figure 8(b)**). Modeled surface DMS falls in the range of the ship measurements. Compared to the aircraft observations, simulated DMS is biased high at the surface and declines more abruptly, which may indicate biases in vertical mixing or cloud processing. DMS concentrations are slightly lower in the simulation with updated chemistry [MOD\_2000], but follow



the same vertical profile. We disaggregate the ATom observations into three regional groups, namely  
445 Pacific, Atlantic, and Southern Oceans as in **Figure 8(a)**. DMS concentrations were measured by two  
instruments during ATom (WAS and TOGA, the former generally reported higher values); both are  
compared with model values in **Figure 8(c)**. Observed DMS concentrations during ATom are  
substantially lower than measured during VOCALS, and lower than any region simulated by the model.  
Modeled DMS is biased high in all three regions, especially over the Southern region where the  
450 discrepancy extends up to 5 km. The new chemistry increases DMS losses and shortens the DMS  
lifetime, reducing the model bias in [MOD\_2000]. The decrease in simulated DMS is largest over the  
Southern Oceans (−49% at the surface), where oxidation by BrO and O<sub>3</sub> in the aqueous phase are  
important and the model-observation bias is substantially reduced. The remaining model biases during  
ATom exceed the uncertainty of the kinetics for the current DMS oxidation scheme and are likely  
455 attributable, at least in part, to the uncertainty in DMS emission. A sensitivity test where we reduce the  
sea surface DMS concentration by 50% in regions south of 30°S in [MOD\_2000] produces, as expected,  
a comparable decrease in DMS mixing ratios in the lower atmosphere (<5 km), and the model-  
observation deviations are further narrowed (see **Figure S4** and **Supplementary Information** for  
details). Constraining DMS emissions is beyond the scope of this work, but is clearly a major source of  
460 uncertainty.

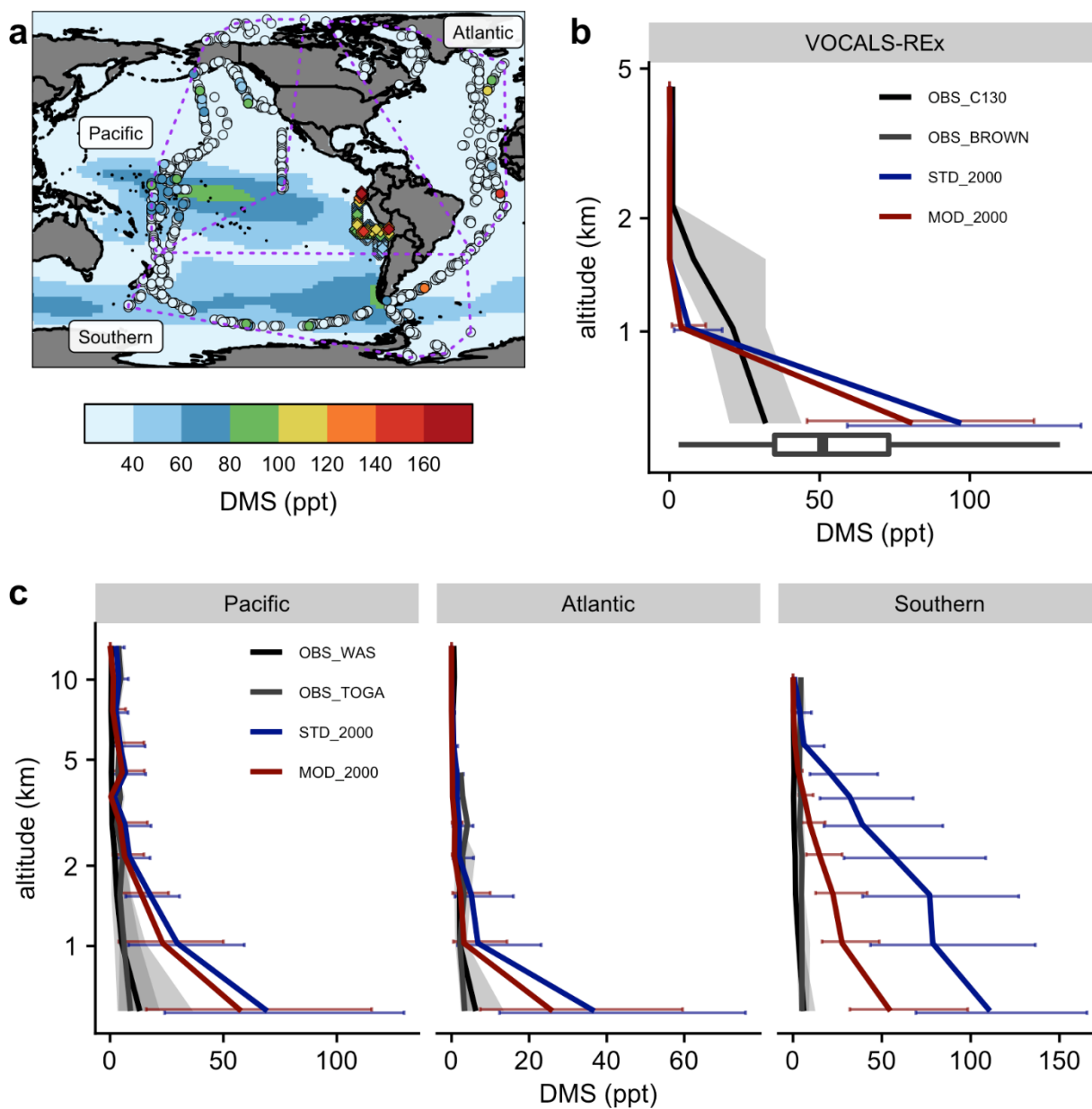




**Figure 8.** (a) Measurements of DMS during VOCALS-REx (diamonds in southeast Pacific near the coastline of Peru) and ATom (dots) missions. Measured values showing are local 90-percentiles above  
465 oceans. ATom data are grouped into three regions as shown in the purple dashed polygons. Marine-  
only annual-mean near-surface (>500 hPa) DMS mixing ratios from [MOD\_2000] are shown in the  
background as a reference. Vertically-binned modeled and observed medians of DMS, during (b)  
VOCALS-REx and (c) ATom, are shown. Error bars and gray shadings indicate data ranged between  
corresponding upper and lower quantiles.

470

**Figure 9** compares the mean vertical profile of HPMTF mixing ratios observed during ATom  
against the model [MOD\_2000]. Over the Pacific and Atlantic regions, HPMTF mixing ratios are  
largest at lower altitudes and decrease to <1 ppt in the middle and upper troposphere. The model  
generally reproduces the observed magnitude and vertical profile. The model [MOD\_2000] is biased  
475 high over the Southern Ocean region, particularly in the lower troposphere. Such high biases are  
consistent with the aforementioned overestimation of DMS over this region. In the lower atmosphere  
over tropical and mid-latitude oceans, the modeled DMS:HPMTF ratios range from 5:1 to 2:1, which  
is larger than the 1:1 ratio observed during ATom (Veres et al., 2020), suggesting that the model may  
underestimate the DMS-to-HPMTF conversion rate or overestimate the HPMTF loss. Our model  
480 predicts that OH-oxidation to SO<sub>2</sub> is dominant in the removal of HPMTF while dry and wet deposition  
are negligible. The addition of cloud uptake (discussed in Sect. 2.3.2) can dramatically decrease  
HPMTF concentration (by up to >73% when assuming moderate cloud uptake rate of  $5 \times 10^{-5} \text{ s}^{-1}$ ),  
resulting in a better model-observation agreement in the lower troposphere over the Southern Ocean  
but low biases over the Pacific and Atlantic (**Figure 9**). In light of the DMS biases of **Figure 8**, this  
485 irreversible cloud uptake may over-correct the HPMTF concentrations.

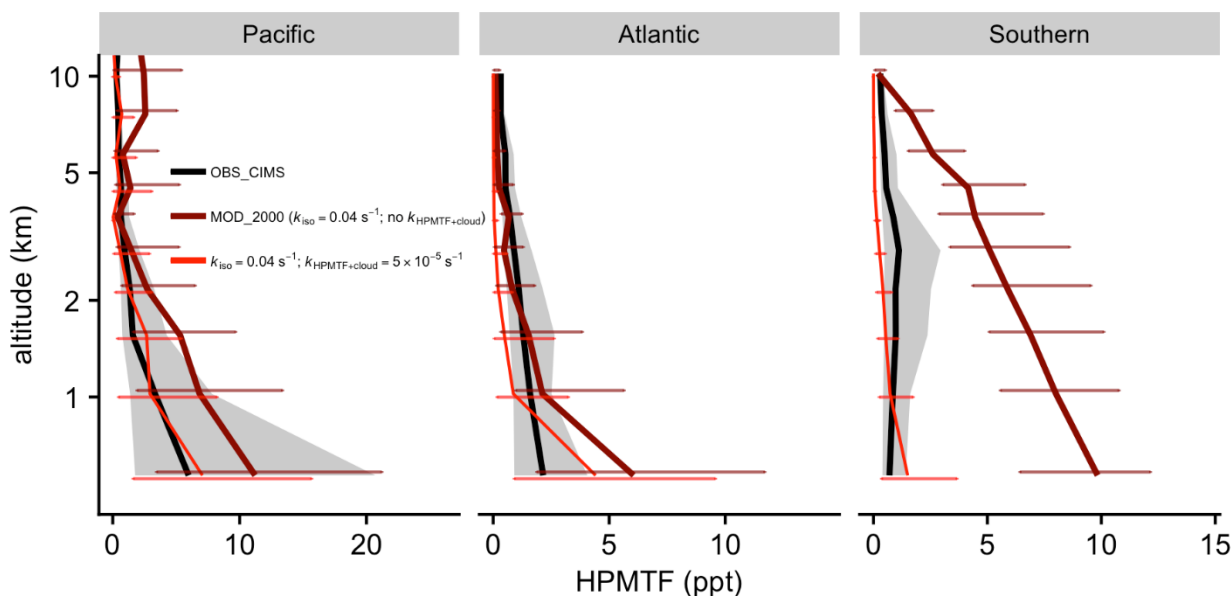


**Figure 9.** Measured (ATom) and modeled values of HPMTF, vertically binned. The thick lines show medians. Error bars and gray shadings indicate data ranged between corresponding upper and lower  
490 quantiles. The thin red line indicates the results from a sensitivity test with  $k_{\text{iso}}$  at  $0.04 \text{ s}^{-1}$  and  $k_{\text{HPMTF+cloud}}$  at  $5 \times 10^{-5} \text{ s}^{-1}$ .

Our simulation shows that the gas-phase MSA formation is small compared to aqueous-phase formation, in line with previous work (Barnes et al., 2006; von Glasow and Crutzen, 2004; Zhu et al.,  
495 2006; Hoffmann et al., 2016; Chen et al., 2018; Hoffmann et al., 2021). Near the sea surface, simulated gas-phase MSA is  $< 0.03 \text{ ppt}$  even in Southern Hemisphere summer, while a recent ship-based measurement reported an averaged concentration ranged 1.4–25 ppt (Yan et al., 2019). The model also substantially underestimates gas-phase MSA ( $< 0.001 \text{ ppt}$ ) when compared to a wintertime site measurements in Germany (0.5–10 ppt) (Stieger et al., 2021). **Figure 10** shows the concentration of  
500 submicron particulate MSA measured during ATom and the collocated concentration of MSA aerosol in Aitken and accumulated modes modeled by [MOD\_2000]. The model overestimates the mid-



505 tropospheric MSA concentrations in the Southern Ocean during ATom. Conversely, over the Pacific and Atlantic, the model underestimates MSA at mid- and low altitudes. Over the southeastern Pacific, the measured submicron MSA from VOCALS-REx ranged from 50–80 ng m<sup>-3</sup> at lower altitudes (<1 km) (Wood et al., 2011) while the location-matched simulated MSA was considerably lower (6–15 ng m<sup>-3</sup>). Above Graciosa Island in the north Atlantic, ACE-ENA-observed MSA ranged from 10–20 ng m<sup>-3</sup> at the lower troposphere (<1 km) and gradually reduced to ~5 ng m<sup>-3</sup> in the mid-troposphere (2–5 km) (Zawadowicz et al., 2021), whereas the model estimates a negligible amount of MSA (<0.5 ng m<sup>-3</sup>) near the Azores, as a result of limited DMS emissions in that region (as reflected by low DMS

510 concentrations in **Figure 2**). Outside of the Southern Ocean, the mean simulated concentration of MSA is underestimated compared to all observations, which suggests that the MSA-forming branches of DMS oxidation (H-abstraction where MSP reacts with NO, or multi-phase OH-addition reactions of DMS) may be under-represented in our simulations, or that the loss of MSA (by reaction with OH, the reaction rate for which is still highly uncertain (Milne et al., 1989; Zhu et al., 2006; Chen et al., 2018))

515 may be overestimated.

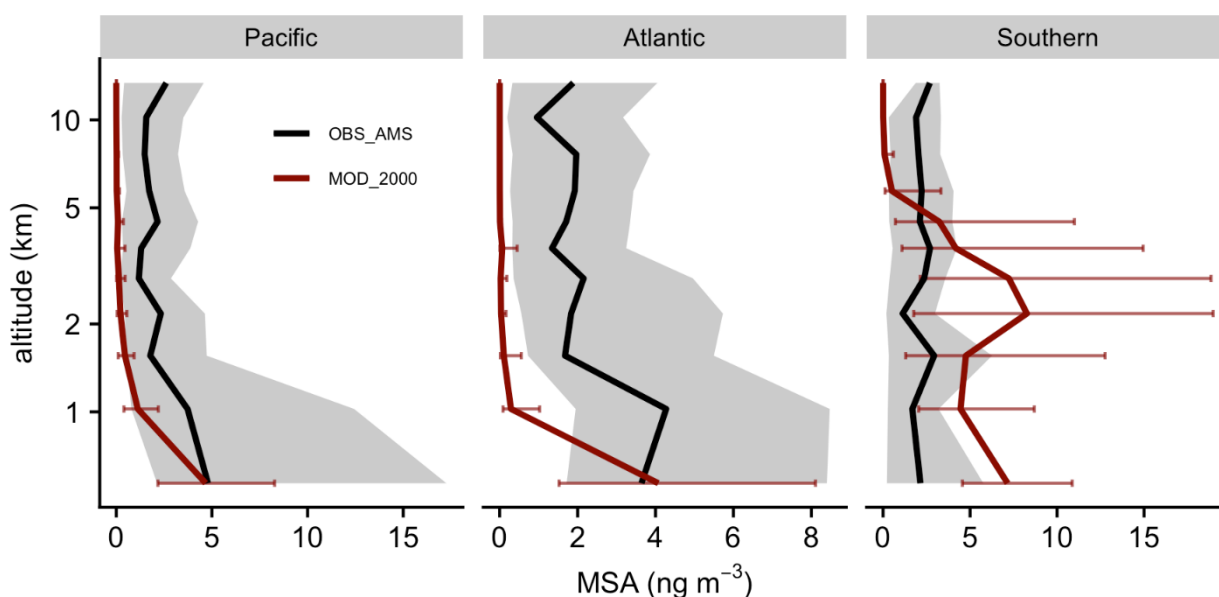




**Figure 10.** Medians of observed (ATom) and modeled concentration of MSA aerosol, vertically binned. The thick lines show medians. Error bars and gray shadings indicate data ranged between corresponding upper and lower quantiles.

Concentrations of the sulfate aerosol simulated with both [STD\_2000] and [MOD\_2000] generally agree well with measurements from ATom (**Figure S6**). Our model also performs well at the surface when compared against VOCAL-REx and ACE-ENA, but is biased high above 1 km, likely reflecting biases in anthropogenic sulfate exported from continental regions.

### 3.3 Global sulfur budget and distribution in the pre-industrial era

As seen under PD conditions, the formation of intermediates expands the overall lifetime of sulfur-containing species in the PI atmosphere, thereby increasing the natural sulfate aerosol background. A summary of the burdens and lifetimes of the sulfur-containing species from the PI simulations is given in **Table S1**. The DMS burden in PI from [MOD\_1850] is 84% larger than its PD counterpart due to slower oxidation which prolongs the atmospheric lifetime. Oxidation by OH via the H-abstraction (38% of total DMS oxidation in [MOD\_1850]) and the OH-addition channels (27%) are still the primary loss pathways of DMS (**Figure S7**). DMS+NO<sub>3</sub> becomes less important (23% in PD vs. 6.0% in PI) given reduced sources of NO<sub>x</sub>, resulting in a lowered DMS-to-SO<sub>2</sub> conversion rate at 27%, compared to 47% in [MOD\_2000] (**Figure S8**). Reduced NO<sub>x</sub> also limits the reaction rates of MSP+NO, thereby favoring the isomerization pathway (92% of total loss of MSP in PD vs. 96% in PI). Hence, the conversion of DMS to HPMTF becomes more important (39% of total DMS oxidation in PI), leading to a doubling of the HPMTF burden in the PI compared to PD. The addition pathway producing MSA becomes more dominant over the tropical ocean via oxidation by OH and the high latitudes by DMS+BrO, raising the MSA burden by 59% compared to PD. Lastly, the expanded DMS oxidation chemistry increases the PI global annual-mean sulfate burden by 29% from 319 Gg-S



[STD\_1850] to 412 Gg-S ([MOD\_1850]) (**Figure 5**), of which 57% is derived from DMS, significantly larger than the 31% in PD, confirming that DMS is a relatively more important source of sulfate in PI. Similar to PD, the majority (66%) of this additional sulfate in the PI is produced via the expanded gas-phase oxidation pathways and this addition is largely aseasonal. The absolute burden of sulfate produced from DMS oxidation is higher in the PI (236 Gg-S) compared to the PD (178 Gg-S).

#### 4 Global Radiative Impacts of Updated DMS Chemistry

Changes to particle-phase sulfate and MSA due to the expanded DMS chemistry, as described above, may alter both aerosol-radiation and aerosol-cloud interactions. Given that particulate MSA is not included in the current CAM6-chem aerosol scheme, to account for its radiative impacts, we assume MSA interacts with radiation like sulfate optically by implementing an artificial rapid conversion of MSA to sulfate. These two adjusted cases are aliased as [MOD\_RE\_1850] and [MOD\_RE\_2000] respectively. Details of this implementation are described in **Supplementary Information**.

##### 4.1 Direct Radiative Effect (DRE)

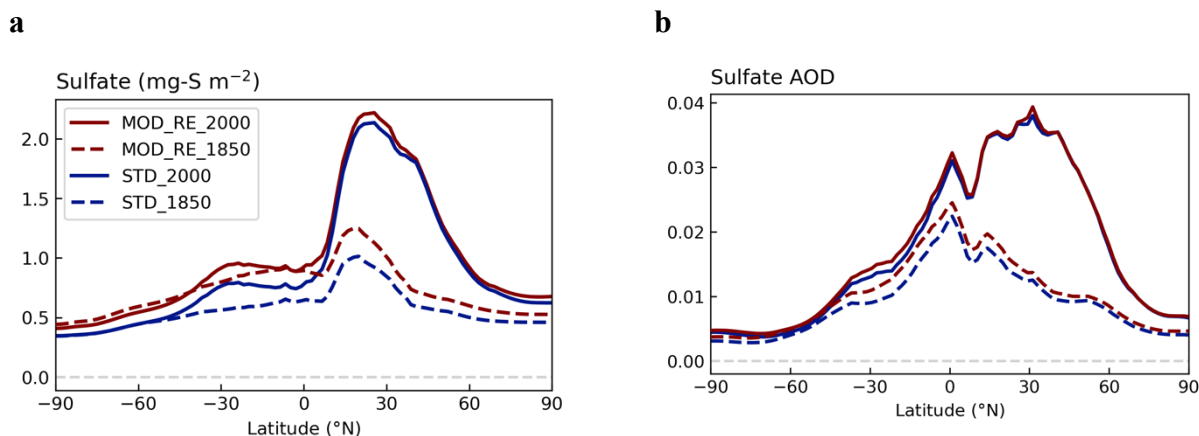
Following the recommendation in Ghan (2013), we focus our analyses on the shortwave (SW) DRE. The PD global annual-mean sulfate DRE modeled with [MOD\_RE\_2000] and [STD\_2000] are  $-0.32 \text{ W m}^{-2}$  and  $-0.31 \text{ W m}^{-2}$ , respectively, which are slightly less negative than previous estimations of  $-0.36 \text{ W m}^{-2}$  to  $-0.42 \text{ W m}^{-2}$  (Heald et al., 2014; Myhre et al., 2013; Yang et al., 2017). The global annual-mean cloud fraction in the model is 77% while the all-sky DRE is 59% of the estimate of clear-sky DRE. The more frequent cloudiness in CAM6-chem may explain the lower DRE compared to the AeroCom II models, which report a typical all-sky to clear-sky ratio of 1:2 (Myhre et al., 2013). The DMS-associated sulfate DRE in PD is  $-0.11 \text{ W m}^{-2}$  in [MOD\_RE\_2000], which is slightly stronger than the value of  $-0.074 \text{ W m}^{-2}$  in a CAM5-chem study using the standard DMS oxidation chemistry (Yang et al., 2017) but substantially weaker than the  $-0.23 \text{ W m}^{-2}$  reported by Rap et al. (2013) using a different model. The DRE contribution of MSA alone is small ( $-0.8 \text{ mW m}^{-2}$ ; estimated by the DRE



difference of [MOD\_RE\_2000] minus [MOD\_2000]). The sulfate DRE is not sensitive to HPMTF cloud loss given that this loss has a modest impact on the sulfate burden in our simulations. Our new  
570 DMS chemistry has strengthened the PD sulfate direct cooling by  $0.01 \text{ W m}^{-2}$  or 4% of the contribution attributed to DMS relative to [STD\_2000].

The rise in sulfate burden from PI to PD driven by anthropogenic emissions occurs mainly over the land in the northern hemisphere; this impact is much larger than the increase in sulfate produced by the expanded DMS chemistry (**Figure 11**). The zonal extrema of PD sulfate burden, aerosol optical  
575 depth (AOD), and DRE are collocated around  $30^\circ\text{N}$  (**Figure 11**). The larger difference in sulfate load in the southern tropics ( $30^\circ\text{S}$  to  $0^\circ\text{N}$ ) due to the new DMS oxidation reactions also translates to a larger DRE difference in those latitudes (**Figure S9**).

The direct radiative forcing (DRF) is estimated by differencing the DRE estimated with anthropogenic emissions at 1850- and 2000-levels. The DRF of [MOD\_RE] and [STD] attributed to  
580 sulfate and MSA aerosols are calculated as  $-0.11 \text{ W m}^{-2}$  and  $-0.13 \text{ W m}^{-2}$ , respectively This difference indicates a relatively linear relationship between sulfate loading and DRF.





c

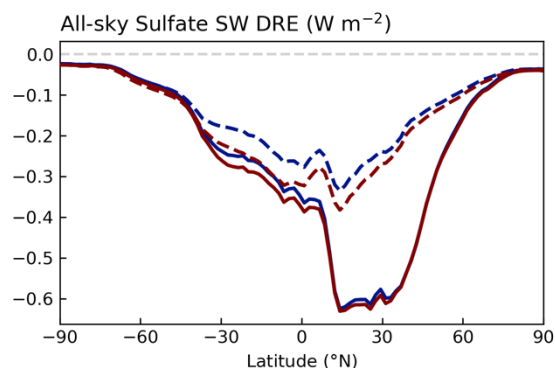


**Figure 11.** Contrasting the zonal-means of (a) sulfate column concentration, (b) sulfate AOD, and (c) all-sky SW sulfate DRE, modeled with [MOD\_RE] and [STD] chemistry at the PI and PD emission levels. Note that particulate MSA is included as sulfate in the MOD\_RE simulations.

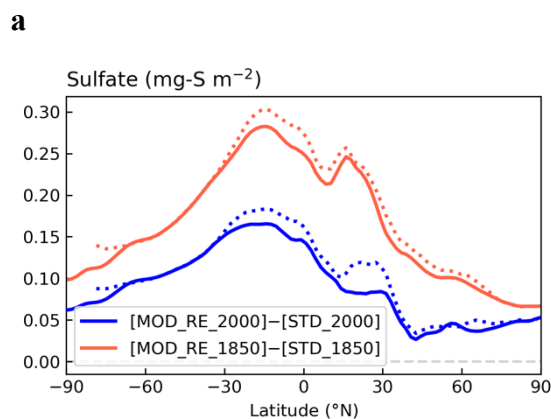
#### 4.2 Impacts on Aerosol-cloud Interactions and Indirect Radiative Forcing (IRF)

585 While the central estimate of the IRF of aerosols from the AR5, which reflects constraints from selected satellite and GCM analyses, is  $-0.45 \text{ W m}^{-2}$ , the IRF estimated by the majority of models reported in AR5 (see Figure 7-19 of Boucher et al. (2013)) ranges from  $-1.0$  to  $-2.5 \text{ W m}^{-2}$ . This suggests that aerosol-cloud interactions may be substantially overestimated by the majority of models; an overly pristine pre-industrial may contribute to this (Menon et al., 2002; Carslaw et al., 2013). We anticipate that the increase in PI sulfate following the expansion of DMS chemistry (**Figure 11a**) may dampen the IRF in our simulations. We evaluate IRF by calculating changes in the SW cloud radiative effects ( $\Delta\text{CRE}$ ) from PI to PD conditions, following previous studies (Gettelman et al., 2019; Ghan, 2013). Our estimates of IRF encapsulate not only the Twomey and the Albrecht effect (Twomey, 1977; Albrecht, 1989), but also cloud feedbacks in response to meteorological changes driven by different sulfate aerosol loadings. For instance, our simulations do not fix air temperature and wind fields. Deeper  
595 sulfate aerosol loadings. For instance, our simulations do not fix air temperature and wind fields. Deeper mixing and stronger turbulence may affect cloud microphysics and limit/promote the precipitation efficiency of clouds, and hence alter cloud lifetime (Gettelman and Sherwood, 2016). These cloud



feedback mechanisms are still poorly constrained and contribute to the uncertainty in CRE estimations in both PI and PD eras.

600 The global-mean  $\Delta$ CRE estimated by differencing [STD\_2000] and [STD\_1850] is  $-2.2 \text{ W m}^{-2}$ , comparable to a previous study using CAM6 (Gettelman et al., 2019) which reported SW  $\Delta$ CRE of  $-2.1 \text{ W m}^{-2}$  with CMIP6 emissions. They also showed that under CMIP5 emissions the magnitude of the SW  $\Delta$ CRE drops to  $-1.4 \text{ W m}^{-2}$ , closer to the AR5 range. Our expanded DMS chemistry leads to a modest ( $\sim 5\%$ ) strengthening in the simulated IRF ( $-2.3 \text{ W m}^{-2}$ ). However, due to the high variability  
605 of the cloud effects, these differences, both in the global values and the zonal means shown in **Figure 12c** are not statistically significant.



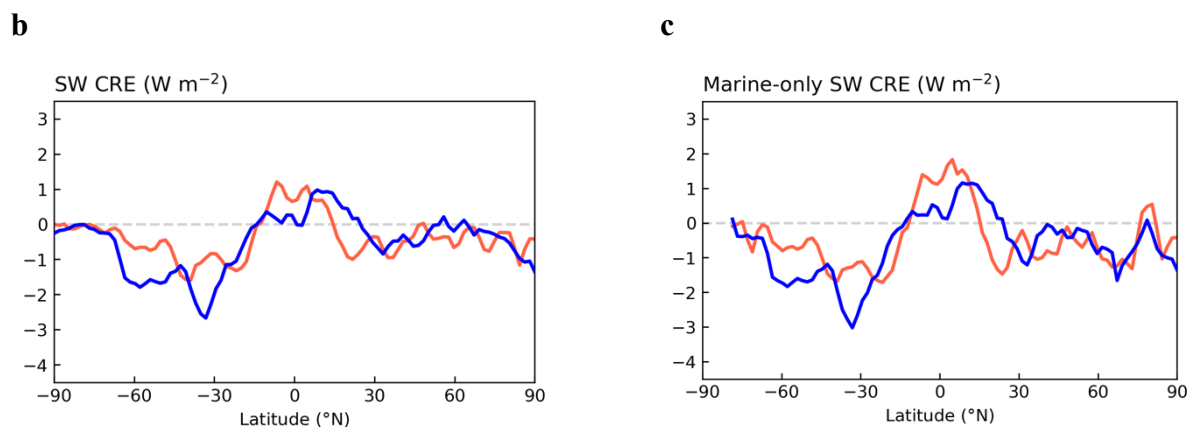


**Figure 12.** Contrasting the zonal-means of changes in (a) sulfate column concentration, (b) SW CRE, and (c) marine-only SW CRE modeled with [MOD\_RE] and [STD] chemistry for PI and PD simulations. Dotted lines in (a) show the zonal mean marine grid cells only.

The strengthening of the IRF is opposite in sign to the expected response to the increase in PI sulfate. Carslaw et al. (2013) describe how cloud albedo is much more strongly sensitive to CCN in the PI, suggesting that higher PI aerosol burden may decrease the cloud response to anthropogenic increases. **Figure 13** illustrates the change of SW CRE and sulfate burden from multiple simulations from PI to PD. Counter to expectations, we find that the SW CRE is more sensitive to each unit increment of sulfate burden (steeper slope) when the PI aerosol burden is higher (in [MOD\_RE], shown in dark red) compared to our baseline simulations ([STD], shown in blue). **Figure S10** shows that the of PI-to-PD change in CCN and cloud properties are also more sensitive to the change in sulfate burden in [MOD\_RE] than [STD]. Hence, each unit PI-to-PD increase in sulfate burden in [MOD\_RE] appears to induce more numerous and smaller cloud droplets and enrich cloud water content, enhancing cloud albedo. This could contribute to the enlarged change in SW CRE (or the IRF) in [MOD\_RE] even though its PI-to-PD sulfate burden increment is smaller than [STD].

This sensitivity may also be related to the spatial distribution in the change in DMS-derived sulfate burden. **Figure 12** shows that the increase in sulfate burden from PI to PD is stronger in the



marine atmosphere, as expected. In a sensitivity test, [GAS\_RE], where only the gas-phase reactions of the new DMS oxidation scheme are enabled but not the aqueous-phase reactions (with the exception of aqueous phase oxidation of SO<sub>2</sub>), produces a less negative IRF of 1.7 W m<sup>-2</sup>. **Figure S11** illustrates that this sensitivity simulation follows the anticipated response, with an increase in PI sulfate decreasing the change in liquid water path (LWP) from PI and PD (particularly in low clouds) and thus dampening the IRF, indicating the important climate implications of marine stratocumulus clouds (Wood, 2012). Contrasting [MOD\_RE] and [GAS\_RE] reveals that the introduction of the aqueous-phase pathway contributes to large changes in the PD-PI sulfate co-located with high clouds over the tropics and low clouds over the Southern Ocean. Though the change in sulfate in both regions produce stronger regional cooling IRF, this appears to be the result of two different processes. In the tropics, decreases in sulfate in the presence of high clouds modify ice nucleation (Gettelman et al., 2010), leading to increased ice water path (IWP) and strengthened cloud cooling over the tropical oceans. Over the Southern Ocean, decreases in sulfate attributable to the aqueous-phase chemistry are associated with even higher LWP in low clouds, further exaggerating the local cooling IRF compared to the gas-phase only simulation. Even though the amount of sulfate produced by the aqueous-phase pathway is relatively small (~8% of DMS-derived sulfate), it appears to have a disproportionate impact on clouds and the estimate of aerosol IRF, suggesting a strong sensitivity of cloud properties to the spatial distribution of natural marine sulfate. More work is needed to better understand this response.

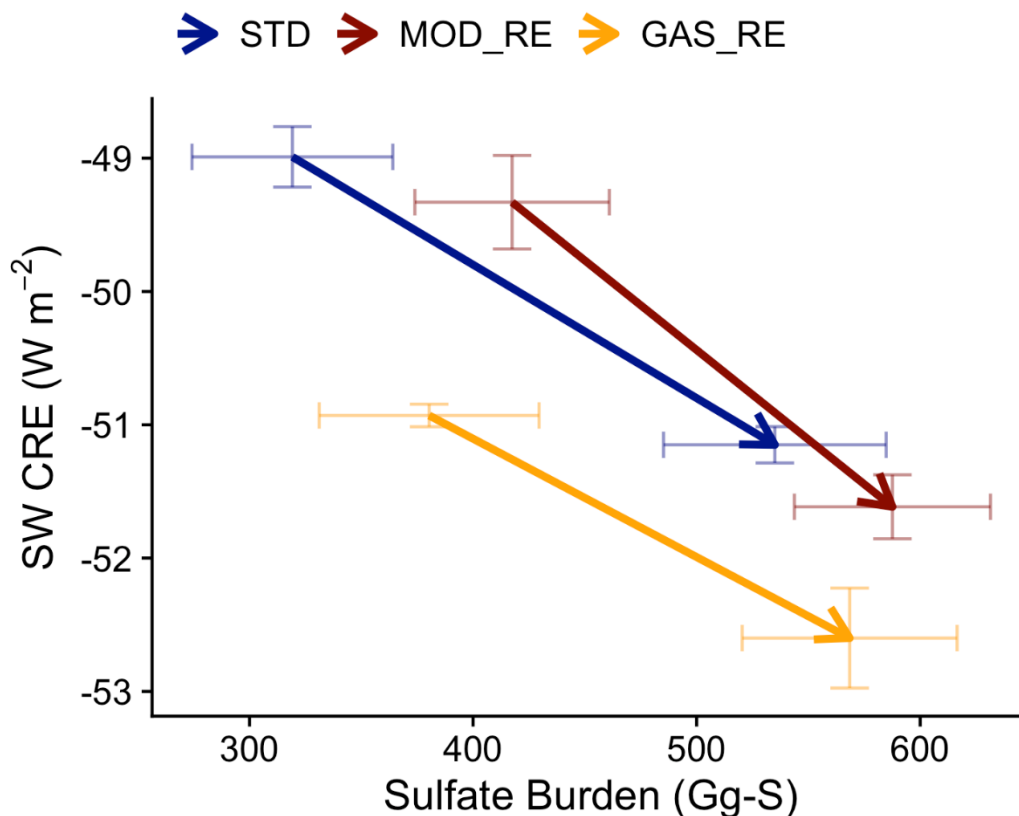


**Figure 13.** PI-to-PD changes in SW CRE and sulfate burden of simulations in this study. [STD] (blue) refers to the simulation with model default chemistry. [MOD\_RE] (dark red) denote the cases with our 645 expanded DMS chemistry implemented with all gas-phase, aerosol-phase, and in-cloud reactions. [GAS\_RE] (yellow) which only includes the expanded gas-phase reactions is also shown. Arrows indicate changes from PI (tails) to PD (heads). Horizontal and vertical error bars span the 1- $\sigma$  variabilities of burden and SW CRE in the simulations, respectively.



## 650 5. Conclusions

We expand the chemical mechanism in CAM6-chem to better describe DMS oxidation in the atmosphere, determine the formation of the intermediate sulfur products, and estimate the aerosol radiative implications under the PI and PD periods.

Uncertainty in our estimate of sulfate response to the new DMS chemistry is largely associated  
655 with estimated reaction rates. Some rate constants for the multiphase reactions are obtained from a limited set of box-model and laboratory studies which have not been validated with field measurements. For example, our rate constant for  $MS_{(aq)}^- + OH_{(aq)}$  from Zhu et al. (2003) is 4.7 times smaller than another lab study (Milne et al., 1989), potentially leading to a higher global tropospheric MSA burden by ~30% (Chen et al., 2018). As discussed in Sect. 3.2, it is likely that our model overestimates the  
660 concentration of particulate MSA and underestimate gaseous MSA when compared with in situ measurements (e.g., ATom, and Yan et al. (2019) in the Southern Ocean. This could result in an overestimate of sulfate given that gas-phase MSA is expected to have a longer lifetime than particulate MSA and  $H_2SO_4$  vapor (Berresheim, 2002). Our comparisons with observations also suggest that emissions of DMS, in particular a likely overestimate over the Southern Ocean, play an important role  
665 in dictating the regional loading of secondary oxidation products

This study included a relatively new chemical mechanism for the formation and loss of HPMTF. The rate of isomerization of MSP ( $k_{iso}$ ) controls the production of HPMTF. The analyses reported here are based on an observationally constrained value of  $k_{iso}$  ( $0.04 \text{ s}^{-1}$  at 293K) (Veres et al., 2020), which is slower than previously experiment- and model-based estimates of  $0.23\text{--}2.1 \text{ s}^{-1}$  (Wu et al., 2015;  
670 Berndt et al., 2019). We find that a faster  $k_{iso}$  ( $0.12 \text{ s}^{-1}$  at 293K based on Ye et al. (2021) has a negligible impact on the HPMTF burden (+4.1%) and resulting sulfate formation. However, the HPMTF burden is quite sensitive to the loss of HPMTF due to cloud uptake ( $k_{HPMTF+cloud}$ ), which was recently suggested as a particularly important sink of HPMTF in the MBL (Veres et al., 2020; Vermeuel et al., 2020). These large changes suggest that further field measurements are needed to better understand the cloud  
675 uptake process of HPMTF and the resulting formation of in-cloud sulfur products.



In this study, we dramatically expand the DMS oxidation mechanism within an Earth System Model. Doing so increases the global sulfate burden by 8.8% in PD, and 29% in PI. While we anticipated that a larger PI burden of sulfate would dampen the aerosol IRF, our simulations instead suggested that the role of aqueous phase chemistry, though modest in terms of the sulfate burden, 680 confounds this effect. In a simulation with only updated gas phase chemistry, the increased PI burden decreased the IRF as anticipated ( $-2.2 \text{ W m}^{-2}$  in standard chemistry vs.  $-1.7 \text{ W m}^{-2}$  with updated gas-phase chemistry). However, high clouds in the tropics and low clouds in the Southern Ocean appear to be particularly sensitive to the sulfate produced via the aqueous phase pathway, counteracting the effect of the additional sulfate formed via the gas-phase pathways (net  $-2.3 \text{ W m}^{-2}$ ). These large differences 685 confirm the high sensitivity of aerosol indirect effects to the natural aerosol background, while revealing complex cloud responses to aerosol produced in different geographical regions via different pathways. More work is needed to understand these responses (e.g., better understanding of cloud responses to aerosols formed in the aqueous phase, observational constraints on the cloud uptake process of HPMTF via both laboratory and field measurements). While our new chemistry increases computational costs 690 by  $\sim 15\%$  (in core-hours/simulation-year), this study suggests that a detailed description of the chemical oxidation of DMS and its products, and particularly the chemistry relevant to pristine conditions, is needed to accurately represent the abundance of natural sulfur species in the marine atmosphere and changes in natural aerosol burden over time.



## 695 **Code availability**

The modified codes of CESM2 developed in this study will be available upon request.

## **Author Contribution**

KMF, CLH and JHK formulated the overarching research goals and aims. KMF and CLH designed the  
700 methodology. KMF implemented the new codes into CAM6-chem based on the standard model  
developed by SW, DJ, AG, ZL, XL, and RAZ. KMF validated the model results against observational  
data provided by EA, DRB, JLJ, PC, PV, TSB, JES, and MZ. KMF analyzed the data and created  
figures. KMF and CLH wrote the initial draft of this manuscript. All authors reviewed this manuscript.

## 705 **Competing Interests**

The authors declare that they have no conflict of interest.

## **Acknowledgment**

This work was supported by U.S. Department of Energy (DOE) (Ref: DE-SC0018934) awarded to CLH  
710 and JHK. RAZ acknowledges support by the U.S. DOE Office of Science, Office of Biological and  
Environmental Research (BER), Earth and Environmental System Modeling (EESM) program as part  
of its Earth System Model Development (ESMD) activity. JLJ and PC were supported by the funding  
from NASA (Ref: 80NSSC18K0630 & 80NSSC19K0124). JES and MAZ were supported by ARM  
and DOE's Atmospheric System Research, an Office of Science Biological and Environmental  
715 Research program. We thank Rebecca Schwantes, Simone Tilmes, and Louisa Emmons for their



contribution to the modeling of this study. This material is based upon work supported by the National Center for Atmospheric Research, which is a major facility sponsored by the NSF under Cooperative Agreement No. 1852977. The high-performance computing was conducted on Cheyenne (doi:10.5065/D6RX99HX) provided by NCAR's Computational and Information Systems Laboratory, 720 sponsored by the National Science Foundation. We also thank Andy Neuman, Alan Bandy, Barry J. Huebert, and Stephen R. Springston for their contribution to the measurements used in this study. ACE-ENA data were obtained from the Atmospheric Radiation Measurement (ARM) User Facility, a U.S. DOE Office of Science user facility managed by the Biological and Environmental Research Program.



## 725 References

- Albrecht, B. A.: Aerosols, Cloud Microphysics, and Fractional Cloudiness, *Science*, 245, 1227–1230, <https://doi.org/10.1126/science.245.4923.1227>, 1989.
- Allen, G., Coe, H., Clarke, A., Bretherton, C., Wood, R., Abel, S. J., Barrett, P., Brown, P., George, R., Freitag, S., McNaughton, C., Howell, S., Shank, L., Kapustin, V., Brekhovskikh, V.,  
730 Kleinman, L., Lee, Y.-N., Springston, S., Toniazzo, T., Krejci, R., Fochesatto, J., Shaw, G., Krecl, P., Brooks, B., McMeeking, G., Bower, K. N., Williams, P. I., Crosier, J., Crawford, I., Connolly, P., Allan, J. D., Covert, D., Bandy, A. R., Russell, L. M., Trembath, J., Bart, M., McQuaid, J. B., Wang, J., and Chand, D.: South East Pacific atmospheric composition and variability sampled along 20° S during VOCALS-REx, *Atmos. Chem. Phys.*, 11, 5237–5262,  
735 <https://doi.org/10.5194/acp-11-5237-2011>, 2011.
- Andreae, M. O.: Ocean-atmosphere interactions in the global biogeochemical sulfur cycle, *Mar. Chem.*, 30, 1–29, [https://doi.org/10.1016/0304-4203\(90\)90059-L](https://doi.org/10.1016/0304-4203(90)90059-L), 1990.
- Andres, R. J. and Kasgnoc, A. D.: A time-averaged inventory of subaerial volcanic sulfur emissions, *J. Geophys. Res.*, 103, 25251–25261, <https://doi.org/10.1029/98JD02091>, 1998.
- 740 Apel, E. C., Hornbrook, R. S., Hills, A. J., Blake, N. J., Barth, M. C., Weinheimer, A., Cantrell, C., Rutledge, S. A., Basarab, B., Crawford, J., Diskin, G., Homeyer, C. R., Campos, T., Flocke, F., Fried, A., Blake, D. R., Brune, W., Pollack, I., Peischl, J., Ryerson, T., Wennberg, P. O., Crouse, J. D., Wisthaler, A., Mikoviny, T., Huey, G., Heikes, B., O’Sullivan, D., and Riemer, D. D.: Upper tropospheric ozone production from lightning NO<sub>x</sub>-impacted convection: Smoke  
745 ingestion case study from the DC3 campaign, *J. Geophys. Res. Atmos.*, 120, 2505–2523, <https://doi.org/10.1002/2014JD022121>, 2015.
- Atkinson, R., Baulch, D. L., Cox, R. A., Crowley, J. N., Hampson, R. F., Hynes, R. G., Jenkin, M. E., Rossi, M. J., and Troe, J.: Evaluated kinetic and photochemical data for atmospheric chemistry: Volume I - gas phase reactions of O<sub>x</sub>, HO<sub>x</sub>, NO<sub>x</sub> and SO<sub>x</sub> species, *Atmos. Chem. Phys.*, 4, 1461–  
750 1738, <https://doi.org/10.5194/acp-4-1461-2004>, 2004.
- Ayers, G. P., Bentley, S. T., Ivey, J. P., and Forgan, B. W.: Dimethylsulfide in marine air at Cape Grim, 41°S, *J. Geophys. Res. Atmos.*, 100, 21013–21021, <https://doi.org/10.1029/95JD02144>, 1995.
- 755 Bardouki, H., Berresheim, H., Vrekoussis, M., Sciare, J., Kouvarakis, G., Oikonomou, K., Schneider, J., and Mihalopoulos, N.: Gaseous (DMS, MSA, SO<sub>2</sub>, H<sub>2</sub>SO<sub>4</sub> and DMSO) and particulate (sulfate and methanesulfonate) sulfur species over the northeastern coast of Crete, *Atmos. Chem. Phys.*, 16, 2003.



- Barnes, I., Hjorth, J., and Mihalopoulos, N.: Dimethyl Sulfide and Dimethyl Sulfoxide and Their Oxidation in the Atmosphere, *Chem. Rev.*, 36, <https://doi.org/10.1021/cr020529+>, 2006.
- 760 Barth, M. C., Rasch, P. J., Kiehl, J. T., Benkovitz, C. M., and Schwartz, S. E.: Sulfur chemistry in the National Center for Atmospheric Research Community Climate Model: Description, evaluation, features, and sensitivity to aqueous chemistry, *J. Geophys. Res.*, 105, 1387–1415, <https://doi.org/10.1029/1999JD900773>, 2000.
- Berglen, T. F.: A global model of the coupled sulfur/oxidant chemistry in the troposphere: The sulfur  
765 cycle, *J. Geophys. Res.*, 109, D19310, <https://doi.org/10.1029/2003JD003948>, 2004.
- Berndt, T., Scholz, W., Mentler, B., Fischer, L., Hoffmann, E. H., Tilgner, A., Hyttinen, N., Prisle, N. L., Hansel, A., and Herrmann, H.: Fast Peroxy Radical Isomerization and OH Recycling in the Reaction of OH Radicals with Dimethyl Sulfide, *J. Phys. Chem. Lett.*, 10, 6478–6483, <https://doi.org/10.1021/acs.jpcclett.9b02567>, 2019.
- 770 Berresheim, H.: Gas-aerosol relationships of H<sub>2</sub> SO<sub>4</sub>, MSA, and OH: Observations in the coastal marine boundary layer at Mace Head, Ireland, *J. Geophys. Res.*, 107, 8100, <https://doi.org/10.1029/2000JD000229>, 2002.
- Booth, M. M. and Powell, D. H.: Trace Organic Analysis by Gas Chromatography with Quadrupole  
775 Mass Spectrometry, in: *Encyclopedia of Analytical Chemistry*, American Cancer Society, <https://doi.org/10.1002/9780470027318.a0876>, 2006.
- Boucher, O., Moulin, C., Belviso, S., Aumont, O., Bopp, L., Cosme, E., von Kuhlmann, R., Lawrence, M. G., Pham, M., Reddy, M. S., Sciare, J., and Venkataraman, C.: DMS atmospheric concentrations and sulphate aerosol indirect radiative forcing: a sensitivity study to the DMS  
780 source representation and oxidation, *Atmos. Chem. Phys.*, 3, 49–65, <https://doi.org/10.5194/acp-3-49-2003>, 2003.
- Boucher, O., Randall, D., Artaxo, P., Bretherton, C., Feingold, G., Forster, P., Kerminen, V.-M., Kondo, Y., Liao, H., and Lohmann, U.: Clouds and aerosols, in: *Climate change 2013: the physical science basis. Contribution of Working Group I to the Fifth Assessment Report of the Intergovernmental Panel on Climate Change*, Cambridge University Press, 571–657, 2013.
- 785 Breider, T. J., Chipperfield, M. P., Richards, N. A. D., Carslaw, K. S., Mann, G. W., and Spracklen, D. V.: Impact of BrO on dimethylsulfide in the remote marine boundary layer: IMPACT OF BRO + DMS IN RMBL, *Geophys. Res. Lett.*, 37, n/a-n/a, <https://doi.org/10.1029/2009GL040868>, 2010.



- 790 Burkholder, J. B., Sander, S. P., Abbatt, J. P. D., Barker, J. R., Huie, R. E., Kolb, C. E., Kurylo, M. J.,  
Orkin, V. L., Wilmouth, D. M., and Wine, P. H.: Chemical kinetics and photochemical data for  
use in atmospheric studies: evaluation number 18, Pasadena, CA: Jet Propulsion Laboratory,  
National Aeronautics and Space Administration, 2015.
- 795 Canagaratna, M. R., Jayne, J. T., Jimenez, J. L., Allan, J. D., Alfarra, M. R., Zhang, Q., Onasch, T. B.,  
Drewnick, F., Coe, H., Middlebrook, A., Delia, A., Williams, L. R., Trimborn, A. M., Northway,  
M. J., DeCarlo, P. F., Kolb, C. E., Davidovits, P., and Worsnop, D. R.: Chemical and  
microphysical characterization of ambient aerosols with the aerodyne aerosol mass spectrometer,  
Mass Spectrometry Rev., 26, 185–222, <https://doi.org/10.1002/mas.20115>, 2007.
- 800 Carn, S. A., Fioletov, V. E., McLinden, C. A., Li, C., and Krotkov, N. A.: A decade of global  
volcanic SO<sub>2</sub> emissions measured from space, Sci Rep, 7, 44095,  
<https://doi.org/10.1038/srep44095>, 2017.
- Carslaw, K. S., Lee, L. A., Reddington, C. L., Pringle, K. J., Rap, A., Forster, P. M., Mann, G. W.,  
Spracklen, D. V., Woodhouse, M. T., Regayre, L. A., and Pierce, J. R.: Large contribution of  
natural aerosols to uncertainty in indirect forcing, Nature, 503, 67–71,  
<https://doi.org/10.1038/nature12674>, 2013.
- 805 Charlson, R. J., Lovelock, J. E., Andreae, M. O., and Warren, S. G.: Oceanic phytoplankton,  
atmospheric sulphur, cloud albedo and climate, Nature, 326, 655–661,  
<https://doi.org/10.1038/326655a0>, 1987.
- 810 Chen, Q., Sherwen, T., Evans, M., and Alexander, B.: DMS oxidation and sulfur aerosol formation in  
the marine troposphere: a focus on reactive halogen and multiphase chemistry, Atmos. Chem.  
Phys., 18, 13617–13637, <https://doi.org/10.5194/acp-18-13617-2018>, 2018.
- Chin, M., Jacob, D. J., Gardner, G. M., Foreman-Fowler, M. S., Spiro, P. A., and Savoie, D. L.: A  
global three-dimensional model of tropospheric sulfate, J Geophys. Res. Atmos., 101, 18667–  
18690, <https://doi.org/10.1029/96JD01221>, 1996.
- 815 Chin, M., Rood, R. B., Lin, S.-J., Müller, J.-F., and Thompson, A. M.: Atmospheric sulfur cycle  
simulated in the global model GOCART: Model description and global properties, J Geophys.  
Res. Atmos., 105, 24671–24687, <https://doi.org/10.1029/2000JD900384>, 2000.
- Cosme, E., Genthon, C., Martinerie, P., Boucher, O., and Pham, M.: The sulfur cycle at high-southern  
latitudes in the LMD-ZT General Circulation Model, J. Geophys. Res. Atmos., 107,  
<https://doi.org/10.1029/2002JD002149>, 2002.



- 820 Danabasoglu, G., Lamarque, J. -F., Bacmeister, J., Bailey, D. A., DuVivier, A. K., Edwards, J.,  
Emmons, L. K., Fasullo, J., Garcia, R., Gettelman, A., Hannay, C., Holland, M. M., Large, W.  
G., Lauritzen, P. H., Lawrence, D. M., Lenaerts, J. T. M., Lindsay, K., Lipscomb, W. H., Mills,  
M. J., Neale, R., Oleson, K. W., Otto-Bliesner, B., Phillips, A. S., Sacks, W., Tilmes, S.,  
Kamphenhout, L., Vertenstein, M., Bertini, A., Dennis, J., Deser, C., Fischer, C., Fox-Kemper, B.,  
825 Kay, J. E., Kinnison, D., Kushner, P. J., Larson, V. E., Long, M. C., Mickelson, S., Moore, J. K.,  
Nienhouse, E., Polvani, L., Rasch, P. J., and Strand, W. G.: The Community Earth System Model  
Version 2 (CESM2), *J. Adv. Model. Earth Syst.*, 12, <https://doi.org/10.1029/2019MS001916>,  
2020.
- 830 Dentener, F. J. and Crutzen, P. J.: Reaction of N<sub>2</sub>O<sub>5</sub> on tropospheric aerosols: Impact on the global  
distributions of NO<sub>x</sub>, O<sub>3</sub>, and OH, *J Geophys. Res. Atmos.*, 98, 7149–7163,  
<https://doi.org/10.1029/92JD02979>, 1993.
- 835 Emmons, L. K., Walters, S., Hess, P. G., Guenther, A., Kinnison, D., Laepple, T., Orlando, J., Tie, X.,  
Tyndall, G., Wiedinmyer, C., Baughcum, S. L., and Kloster, S.: Description and evaluation of the  
Model for Ozone and Related chemical Tracers, version 4 (MOZART-4), *Geosci. Model Dev.*,  
25, 2010.
- 840 Emmons, L. K., Schwantes, R. H., Orlando, J. J., Tyndall, G., Kinnison, D., Lamarque, J., Marsh, D.,  
Mills, M. J., Tilmes, S., Bardeen, C., Buchholz, R. R., Conley, A., Gettelman, A., Garcia, R.,  
Simpson, I., Blake, D. R., Meinardi, S., and Pétron, G.: The Chemistry Mechanism in the  
Community Earth System Model Version 2 (CESM2), *J. Adv. Model. Earth Syst.*, 12,  
<https://doi.org/10.1029/2019MS001882>, 2020.
- Enami, S., Nakano, Y., Hashimoto, S., Kawasaki, M., Aloisio, S., and Francisco, J. S.: Reactions of  
Cl atoms with dimethyl sulfide: A theoretical calculation and an experimental study with cavity  
ring-down spectroscopy, *J. Phys. Chem. A*, 108, 7785–7789, 2004.
- 845 Fahey, K. M., Carlton, A. G., Pye, H. O. T., Baik, J., Hutzell, W. T., Stanier, C. O., Baker, K. R.,  
Appel, K. W., Jaoui, M., and Offenberg, J. H.: A framework for expanding aqueous chemistry in  
the Community Multiscale Air Quality (CMAQ) model version 5.1, *Geosci. Model Dev.*, 10,  
1587–1605, <https://doi.org/10.5194/gmd-10-1587-2017>, 2017.
- 850 Faloon, I.: Sulfur processing in the marine atmospheric boundary layer: A review and critical  
assessment of modeling uncertainties, *Atmospheric Environment*, 43, 2841–2854,  
<https://doi.org/10.1016/j.atmosenv.2009.02.043>, 2009.
- Flyunt, R., Makogon, O., Schuchmann, M. N., Asmus, K.-D., and von Sonntag, C.: OH-Radical-  
induced oxidation of methanesulfinic acid. The reactions of the methanesulfonyl radical in the  
absence and presence of dioxygen, *J. Chem. Soc., Perkin Trans. 2*, 787–792,  
<https://doi.org/10.1039/b009631h>, 2001.



- 855 Gershenson, M., Davidovits, P., Jayne, J. T., Kolb, C. E., and Worsnop, D. R.: Simultaneous Uptake of DMS and Ozone on Water, *J. Phys. Chem. A*, 105, 7031–7036, <https://doi.org/10.1021/jp010696y>, 2001.
- Gettelman, A.: Putting the clouds back in aerosol–cloud interactions, *Atmos. Chem. Phys.*, 15, 12397–12411, <https://doi.org/10.5194/acp-15-12397-2015>, 2015.
- 860 Gettelman, A. and Sherwood, S. C.: Processes Responsible for Cloud Feedback, *Curr Clim Change Rep*, 2, 179–189, <https://doi.org/10.1007/s40641-016-0052-8>, 2016.
- Gettelman, A., Liu, X., Ghan, S. J., Morrison, H., Park, S., Conley, A. J., Klein, S. A., Boyle, J., Mitchell, D. L., and Li, J.-L. F.: Global simulations of ice nucleation and ice supersaturation with an improved cloud scheme in the Community Atmosphere Model, *J. Geophys. Res.*, 115, D18216, <https://doi.org/10.1029/2009JD013797>, 2010.
- 865
- Gettelman, A., Hannay, C., Bacmeister, J. T., Neale, R. B., Pendergrass, A. G., Danabasoglu, G., Lamarque, J. -F., Fasullo, J. T., Bailey, D. A., Lawrence, D. M., and Mills, M. J.: High Climate Sensitivity in the Community Earth System Model Version 2 (CESM2), *Geophys. Res. Lett.*, 46, 8329–8337, <https://doi.org/10.1029/2019GL083978>, 2019.
- 870 Ghan, S. J.: Technical Note: Estimating aerosol effects on cloud radiative forcing, *Atmos. Chem. Phys.*, 13, 9971–9974, <https://doi.org/10.5194/acp-13-9971-2013>, 2013.
- von Glasow, R. and Crutzen, P. J.: Model study of multiphase DMS oxidation with a focus on halogens, *Atmos. Chem. Phys.*, 4, 589–608, <https://doi.org/10.5194/acp-4-589-2004>, 2004.
- Gondwe, M., Krol, M., Gieskes, W., Klaassen, W., and de Baar, H.: The contribution of ocean-leaving DMS to the global atmospheric burdens of DMS, MSA, SO<sub>2</sub>, and NSS SO<sub>4</sub><sup>−</sup>, *Global Biogeochem. Cycles*, 17, <https://doi.org/10.1029/2002GB001937>, 2003.
- 875
- Guenther, A. B., Jiang, X., Heald, C. L., Sakulyanontvittaya, T., Duhl, T., Emmons, L. K., and Wang, X.: The Model of Emissions of Gases and Aerosols from Nature version 2.1 (MEGAN2.1): an extended and updated framework for modeling biogenic emissions, *Geosci. Model Dev.*, 5, 1471–1492, <https://doi.org/10.5194/gmd-5-1471-2012>, 2012.
- 880
- Heald, C. L., Ridley, D. A., Kroll, J. H., Barrett, S. R. H., Cady-Pereira, K. E., Alvarado, M. J., and Holmes, C. D.: Contrasting the direct radiative effect and direct radiative forcing of aerosols, *Atmos. Chem. Phys.*, 14, 5513–5527, <https://doi.org/10.5194/acp-14-5513-2014>, 2014.
- Hezel, P. J., Alexander, B., Bitz, C. M., Steig, E. J., Holmes, C. D., Yang, X., and Sciare, J.: Modeled methanesulfonic acid (MSA) deposition in Antarctica and its relationship to sea ice, *J. Geophys. Res.*, 116, <https://doi.org/10.1029/2011JD016383>, 2011.
- 885



- 890 Hoesly, R. M., Smith, S. J., Feng, L., Klimont, Z., Janssens-Maenhout, G., Pitkanen, T., Seibert, J. J., Vu, L., Andres, R. J., Bolt, R. M., Bond, T. C., Dawidowski, L., Kholod, N., Kurokawa, J., Li, M., Liu, L., Lu, Z., Moura, M. C. P., O'Rourke, P. R., and Zhang, Q.: Historical (1750–2014) anthropogenic emissions of reactive gases and aerosols from the Community Emissions Data System (CEDS), *Geosci. Model Dev.*, 11, 369–408, <https://doi.org/10.5194/gmd-11-369-2018>, 2018.
- 895 Hoffmann, E. H., Tilgner, A., Schrödner, R., Brüner, P., Wolke, R., and Herrmann, H.: An advanced modeling study on the impacts and atmospheric implications of multiphase dimethyl sulfide chemistry, *Proc Natl Acad Sci USA*, 113, 11776–11781, <https://doi.org/10.1073/pnas.1606320113>, 2016.
- Hoffmann, E. H., Heinold, B., Kubin, A., Tegen, I., and Herrmann, H.: The Importance of the Representation of DMS Oxidation in Global Chemistry-Climate Simulations, *Geophys Res Lett*, 48, <https://doi.org/10.1029/2021GL094068>, 2021.
- 900 Huebert, B. J., Blomquist, B. W., Hare, J. E., Fairall, C. W., Johnson, J. E., and Bates, T. S.: Measurement of the sea-air DMS flux and transfer velocity using eddy correlation, *Geophys. Res. Lett.*, 31, <https://doi.org/10.1029/2004GL021567>, 2004.
- 905 Hurrell, J. W., Hack, J. J., Shea, D., Caron, J. M., and Rosinski, J.: A new sea surface temperature and sea ice boundary dataset for the community atmosphere model, 21, 5145–5153, <https://doi.org/10.1175/2008JCLI2292.1>, 2008.
- Jeffery, C. D., Robinson, I. S., and Woolf, D. K.: Tuning a physically-based model of the air–sea gas transfer velocity, *Ocean Modelling*, 31, 28–35, <https://doi.org/10.1016/j.ocemod.2009.09.001>, 2010.
- 910 Johnson, M. T.: A numerical scheme to calculate temperature and salinity dependent air-water transfer velocities for any gas, *Ocean Sci.*, 6, 913–932, <https://doi.org/10.5194/os-6-913-2010>, 2010.
- Kaufman, Y. J. and Tanré, D.: Effect of variations in super-saturation on the formation of cloud condensation nuclei, *Nature*, 369, 45–48, <https://doi.org/10.1038/369045a0>, 1994.
- 915 Kettle, A. J., Andreae, M. O., Amouroux, D., Andreae, T. W., Bates, T. S., Berresheim, H., Bingemer, H., Boniforti, R., Curran, M. A. J., DiTullio, G. R., Helas, G., Jones, G. B., Keller, M. D., Kiene, R. P., Leck, C., Levasseur, M., Malin, G., Maspero, M., Matrai, P., McTaggart, A. R., Mihalopoulos, N., Nguyen, B. C., Novo, A., Putaud, J. P., Rapsomanikis, S., Roberts, G., Schebeske, G., Sharma, S., Simó, R., Staubes, R., Turner, S., and Uher, G.: A global database of sea surface dimethylsulfide (DMS) measurements and a procedure to predict sea surface DMS as a function of latitude, longitude, and month, *Global Biogeochem. Cycles*, 13, 399–444, <https://doi.org/10.1029/1999GB900004>, 1999.
- 920



- 925 Khan, M. A. H., Gillespie, S. M. P., Razis, B., Xiao, P., Davies-Coleman, M. T., Percival, C. J., Derwent, R. G., Dyke, J. M., Ghosh, M. V., Lee, E. P. F., and Shallcross, D. E.: A modelling study of the atmospheric chemistry of DMS using the global model, STOCHEM-CRI, *Atmospheric Environment*, 127, 69–79, <https://doi.org/10.1016/j.atmosenv.2015.12.028>, 2016.
- 930 Kilgour, D. B., Novak, G. A., Sauer, J. S., Moore, A. N., Dinasquet, J., Amiri, S., Franklin, E. B., Mayer, K., Winter, M., Morris, C. K., Price, T., Malfatti, F., Crocker, D. R., Lee, C., Cappa, C. D., Goldstein, A. H., Prather, K. A., and Bertram, T. H.: Marine gas-phase sulfur emissions during an induced phytoplankton bloom, *Atmos. Chem. Phys.*, 1–24, <https://doi.org/10.5194/acp-2021-615>, 2021.
- Kloster, S., Feichter, J., Maier-Reimer, E., Six, K. D., Stier, P., and Wetzell, P.: DMS cycle in the marine ocean-atmosphere system – a global model study, *Biogeosciences*, 23, 2006.
- Kulmala, M., Pirjola, L., and Mäkelä, J.: Stable sulfate clusters as a source of new atmospheric particles, *Nature*, 404, 66–9, <https://doi.org/10.1038/35003550>, 2000.
- 935 Lamarque, J.-F., Emmons, L. K., Hess, P. G., Kinnison, D. E., Tilmes, S., Vitt, F., Heald, C. L., Holland, E. A., Lauritzen, P. H., Neu, J., Orlando, J. J., Rasch, P. J., and Tyndall, G. K.: CAM-chem: description and evaluation of interactive atmospheric chemistry in the Community Earth System Model, *Geosci. Model Dev.*, 5, 369–411, <https://doi.org/10.5194/gmd-5-369-2012>, 2012.
- 940 Lana, A., Bell, T. G., Simó, R., Vallina, S. M., Ballabrera-Poy, J., Kettle, A. J., Dachs, J., Bopp, L., Saltzman, E. S., Stefels, J., Johnson, J. E., and Liss, P. S.: An updated climatology of surface dimethylsulfide concentrations and emission fluxes in the global ocean, *Global Biogeochem. Cycles*, 25, <https://doi.org/10.1029/2010GB003850>, 2011.
- 945 Lennartz, S. T., Krysztofiak, G., Marandino, C. A., Sinnhuber, B.-M., Tegtmeier, S., Ziska, F., Hossaini, R., Krüger, K., Montzka, S. A., Atlas, E., Oram, D. E., Keber, T., Bönisch, H., and Quack, B.: Modelling marine emissions and atmospheric distributions of halocarbons and dimethyl sulfide: the influence of prescribed water concentration vs. prescribed emissions, *Atmos. Chem. Phys.*, 15, 11753–11772, <https://doi.org/10.5194/acp-15-11753-2015>, 2015.
- 950 Liu, X., Easter, R. C., Ghan, S. J., Zaveri, R., Rasch, P., Shi, X., Lamarque, J.-F., Gettelman, A., Morrison, H., Vitt, F., Conley, A., Park, S., Neale, R., Hannay, C., Ekman, A. M. L., Hess, P., Mahowald, N., Collins, W., Iacono, M. J., Bretherton, C. S., Flanner, M. G., and Mitchell, D.: Toward a minimal representation of aerosols in climate models: description and evaluation in the Community Atmosphere Model CAM5, *Geosci. Model Dev.*, 5, 709–739, <https://doi.org/10.5194/gmd-5-709-2012>, 2012.



- 955 Liu, X., Ma, P.-L., Wang, H., Tilmes, S., Singh, B., Easter, R. C., Ghan, S. J., and Rasch, P. J.:  
Description and evaluation of a new four-mode version of the Modal Aerosol Module (MAM4)  
within version 5.3 of the Community Atmosphere Model, *Geosci. Model Dev.*, 9, 505–522,  
<https://doi.org/10.5194/gmd-9-505-2016>, 2016.
- 960 Lu, Z., Liu, X., Zaveri, R. A., Easter, R. C., Tilmes, S., Emmons, L. K., Vitt, F., Singh, B., Wang, H.,  
Zhang, R., and Rasch, P. J.: Radiative Forcing of Nitrate Aerosols From 1975 to 2010 as  
Simulated by MOSAIC Module in CESM2-MAM4, *Geophys Res Atmos*, 126,  
<https://doi.org/10.1029/2021JD034809>, 2021.
- Lucas, D. D.: Mechanistic studies of dimethylsulfide oxidation products using an observationally  
constrained model, *J. Geophys. Res.*, 107, 4201, <https://doi.org/10.1029/2001JD000843>, 2002.
- 965 Mackay, Donald. and Yeun, A. T. K.: Mass transfer coefficient correlations for volatilization of  
organic solutes from water, *Environ. Sci. Technol.*, 17, 211–217,  
<https://doi.org/10.1021/es00110a006>, 1983.
- 970 van Marle, M. J. E., Kloster, S., Magi, B. I., Marlon, J. R., Daniau, A.-L., Field, R. D., Arneth, A.,  
Forrest, M., Hantson, S., Kehrwald, N. M., Knorr, W., Lasslop, G., Li, F., Mangeon, S., Yue, C.,  
Kaiser, J. W., and van der Werf, G. R.: Historic global biomass burning emissions for CMIP6  
(BB4CMIP) based on merging satellite observations with proxies and fire models (1750–2015),  
*Geosci. Model Dev.*, 10, 3329–3357, <https://doi.org/10.5194/gmd-10-3329-2017>, 2017.
- 975 Meinshausen, M., Vogel, E., Nauels, A., Lorbacher, K., Meinshausen, N., Etheridge, D. M., Fraser, P.  
J., Montzka, S. A., Rayner, P. J., Trudinger, C. M., Krummel, P. B., Beyerle, U., Canadell, J. G.,  
Daniel, J. S., Enting, I. G., Law, R. M., Lunder, C. R., O’Doherty, S., Prinn, R. G., Reimann, S.,  
Rubino, M., Velders, G. J. M., Vollmer, M. K., Wang, R. H. J., and Weiss, R.: Historical  
greenhouse gas concentrations for climate modelling (CMIP6), *Geosci. Model Dev.*, 10, 2057–  
2116, <https://doi.org/10.5194/gmd-10-2057-2017>, 2017.
- 980 Menon, S., Genio, A. D. D., Koch, D., and Tselioudis, G.: GCM simulations of the aerosol indirect  
effect: Sensitivity to cloud parameterization and aerosol burden, *J. Atmos. Chem.*, 59, 692–713,  
2002.
- Mills, M. J., Schmidt, A., Easter, R., Solomon, S., Kinnison, D. E., Ghan, S. J., Neely, R. R., Marsh,  
D. R., Conley, A., Bardeen, C. G., and Gettelman, A.: Global volcanic aerosol properties derived  
from emissions, 1990-2014, using CESM1(WACCM), *J. Geophys. Res. Atmos.*, 121, 2332–  
2348, <https://doi.org/10.1002/2015JD024290>, 2016.
- 985 Milne, P. J., Zika, R. G., and Saltzman, E. S.: Rate of Reaction of Methanesulfonic Acid, Dimethyl  
Sulfoxide, and Dimethyl Sulfone with Hydroxyl Radical in Aqueous Solution, in: *Biogenic  
Sulfur in the Environment*, vol. 393, American Chemical Society, 518–528,  
<https://doi.org/10.1021/bk-1989-0393.ch033>, 1989.



- 990 Miyazaki, K., Eskes, H. J., and Sudo, K.: Global NO<sub>x</sub> emission estimates derived from an assimilation  
of OMI tropospheric NO<sub>2</sub> columns, *Atmos. Chem. Phys.*, 12, 2263–2288,  
<https://doi.org/10.5194/acp-12-2263-2012>, 2012.
- 995 Myhre, G., Shindell, D., Bréon, F.-M., Collins, W., Fuglestedt, J., Huang, J., Koch, D., Lamarque,  
J.-F., Lee, D., Mendoza, B., Nakajima, T., Robock, A., Stephens, G., Zhang, H., Aamaas, B.,  
Boucher, O., Dalsøren, S. B., Daniel, J. S., Forster, P., Granier, C., Haigh, J., Hodnebrog, Ø.,  
Kaplan, J. O., Marston, G., Nielsen, C. J., O'Neill, B. C., Peters, G. P., Pongratz, J., Ramaswamy,  
V., Roth, R., Rotstain, L., Smith, S. J., Stevenson, D., Vernier, J.-P., Wild, O., Young, P., Jacob,  
D., Ravishankara, A. R., and Shine, K.: 8 Anthropogenic and Natural Radiative Forcing, 82,  
2013.
- 1000 Nightingale, P. D., Malin, G., Law, C. S., Watson, A. J., Liss, P. S., Liddicoat, M. I., Boutin, J., and  
Upstill-Goddard, R. C.: In situ evaluation of air-sea gas exchange parameterizations using novel  
conservative and volatile tracers, *Global Biogeochem. Cycles*, 14, 373–387,  
<https://doi.org/10.1029/1999GB900091>, 2000.
- 1005 Patroescu, I. V., Barnes, I., and Becker, K. H.: FTIR Kinetic and Mechanistic Study of the  
Atmospheric Chemistry of Methyl Thiolfornate, 100, 17207–17217,  
<https://doi.org/10.1021/jp961452u>, 1996.
- Pham, M., Müller, J.-F., Brasseur, G. P., Granier, C., and Mégie, G.: A three-dimensional study of the  
tropospheric sulfur cycle, *J. Geophys. Res.*, 100, 26061, <https://doi.org/10.1029/95JD02095>,  
1995.
- 1010 Rap, A., Scott, C. E., Spracklen, D. V., Bellouin, N., Forster, P. M., Carslaw, K. S., Schmidt, A., and  
Mann, G.: Natural aerosol direct and indirect radiative effects, *Geophys. Res. Lett.*, 40, 3297–  
3301, <https://doi.org/10.1002/grl.50441>, 2013.
- 1015 Saunders, S. M., Jenkin, M. E., Derwent, R. G., and Pilling, M. J.: Protocol for the development of  
the Master Chemical Mechanism, MCM v3 (Part A): tropospheric degradation of non-aromatic  
volatile organic compounds, *Atmos. Chem. Phys.*, 3, 161–180, [https://doi.org/10.5194/acp-3-  
161-2003](https://doi.org/10.5194/acp-3-161-2003), 2003.
- Sciare, J., Mihalopoulos, N., and Dentener, F. J.: Interannual variability of atmospheric  
dimethylsulfide in the southern Indian Ocean, *J. Geophys. Res.*, 105, 26369–26377,  
<https://doi.org/10.1029/2000JD900236>, 2000.
- 1020 Sehested, K. and Holcman, J.: A pulse radiolysis study of the OH radical induced autoxidation of  
methanesulfinic acid, *Radiation Physics and Chemistry*, 47, 357–360,  
[https://doi.org/10.1016/0969-806X\(95\)00115-E](https://doi.org/10.1016/0969-806X(95)00115-E), 1996.



- Simpson, I. J., Colman, J. J., Swanson, A. L., Bandy, A. R., Thornton, D. C., Blake, D. R., and Rowland, F. S.: Aircraft measurements of dimethyl sulfide (DMS) using a whole air sampling technique, 39, 191–213, <https://doi.org/10.1023/A:1010608529779>, 2001.
- 1025 Spracklen, D. V., Pringle, K. J., Carslaw, K. S., Chipperfield, M. P., and Mann, G. W.: A global off-line model of size-resolved aerosol microphysics: I. Model development and prediction of aerosol properties, *Atmos. Chem. Phys.*, 26, 2005.
- 1030 Stieger, B., van Pinxteren, D., Tilgner, A., Spindler, G., Poulain, L., Grüner, A., Wallasch, M., and Herrmann, H.: Strong Deviations from Thermodynamically Expected Phase Partitioning of Low-Molecular-Weight Organic Acids during One Year of Rural Measurements, *ACS Earth Space Chem.*, 5, 500–515, <https://doi.org/10.1021/acsearthspacechem.0c00297>, 2021.
- 1035 Tilmes, S., Hodzic, A., Emmons, L. K., Mills, M. J., Gettelman, A., Kinnison, D. E., Park, M., Lamarque, J. -F., Vitt, F., Shrivastava, M., Campuzano-Jost, P., Jimenez, J. L., and Liu, X.: Climate Forcing and Trends of Organic Aerosols in the Community Earth System Model (CESM2), *J. Adv. Model. Earth Syst.*, 11, 4323–4351, <https://doi.org/10.1029/2019MS001827>, 2019.
- Twomey, S.: The Influence of Pollution on the Shortwave Albedo of Clouds, *J. of Atmos. Sci.*, 34, 1149–1152, 1977.
- 1040 Veres, P. R., Neuman, J. A., Bertram, T. H., Assaf, E., Wolfe, G. M., Williamson, C. J., Weinzierl, B., Tilmes, S., Thompson, C. R., Thames, A. B., Schroder, J. C., Saiz-Lopez, A., Rollins, A. W., Roberts, J. M., Price, D., Peischl, J., Nault, B. A., Møller, K. H., Miller, D. O., Meinardi, S., Li, Q., Lamarque, J.-F., Kupc, A., Kjaergaard, H. G., Kinnison, D., Jimenez, J. L., Jernigan, C. M., Hornbrook, R. S., Hills, A., Dollner, M., Day, D. A., Cuevas, C. A., Campuzano-Jost, P., Burkholder, J., Bui, T. P., Brune, W. H., Brown, S. S., Brock, C. A., Bourgeois, I., Blake, D. R., 1045 Apel, E. C., and Ryerson, T. B.: Global airborne sampling reveals a previously unobserved dimethyl sulfide oxidation mechanism in the marine atmosphere, *Proc Natl Acad Sci USA*, 117, 4505–4510, <https://doi.org/10.1073/pnas.1919344117>, 2020.
- 1050 Vermeuel, M. P., Novak, G. A., Jernigan, C. M., and Bertram, T. H.: Diel Profile of Hydroperoxymethyl Thioformate: Evidence for Surface Deposition and Multiphase Chemistry, *Environ. Sci. Technol.*, 54, 12521–12529, <https://doi.org/10.1021/acs.est.0c04323>, 2020.
- Wang, J., Wood, R., Jensen, M., Azevedo, E., Bretherton, C., and Chand, D.: Aerosol and Cloud Experiments in Eastern North Atlantic (ACE-ENA) Field Campaign Report, 18, 2019a.



- 1055 Wang, J., Wood, R., Jensen, M. P., Chiu, J. C., Liu, Y., Lamer, K., Desai, N., Giangrande, S. E.,  
Knopf, D. A., Kollias, P., Laskin, A., Liu, X., Lu, C., Mechem, D., Mei, F., Starzec, M.,  
Tomlinson, J., Wang, Y., Yum, S. S., Zheng, G., Aiken, A. C., Azevedo, E. B., Blanchard, Y.,  
China, S., Dong, X., Gallo, F., Gao, S., Ghate, V. P., Glienke, S., Goldberger, L., Hardin, J. C.,  
Kuang, C., Luke, E. P., Matthews, A. A., Miller, M. A., Moffet, R., Pekour, M., Schmid, B.,  
1060 Sedlacek, A. J., Shaw, R. A., Shilling, J. E., Sullivan, A., Suski, K., Veghte, D. P., Weber, R.,  
Wyant, M., Yeom, J., Zawadowicz, M., and Zhang, Z.: Aerosol and Cloud Experiments in the  
Eastern North Atlantic (ACE-ENA), *Bulletin of the American Meteorological Society*, 1, 1–51,  
<https://doi.org/10.1175/BAMS-D-19-0220.1>, 2021.
- 1065 Wang, S., Hornbrook, R. S., Hills, A., Emmons, L. K., Tilmes, S., Lamarque, J., Jimenez, J. L.,  
Campuzano-Jost, P., Nault, B. A., Crounse, J. D., Wennberg, P. O., Kim, M., Allen, H., Ryerson,  
T. B., Thompson, C. R., Peischl, J., Moore, F., Nance, D., Hall, B., Elkins, J., Tanner, D., Huey,  
L. G., Hall, S. R., Ullmann, K., Orlando, J. J., Tyndall, G. S., Flocke, F. M., Ray, E., Hanisco, T.  
F., Wolfe, G. M., St. Clair, J., Commane, R., Daube, B., Barletta, B., Blake, D. R., Weinzierl, B.,  
Dollner, M., Conley, A., Vitt, F., Wofsy, S. C., Riemer, D. D., and Apel, E. C.: Atmospheric  
1070 Acetaldehyde: Importance of Air-Sea Exchange and a Missing Source in the Remote  
Troposphere, *Geophys. Res. Lett.*, 46, 5601–5613, <https://doi.org/10.1029/2019GL082034>,  
2019b.
- 1075 Wang, S., Kinnison, D., Montzka, S. A., Apel, E. C., Hornbrook, R. S., Hills, A. J., Blake, D. R.,  
Barletta, B., Meinardi, S., Sweeney, C., Moore, F., Long, M., Saiz-Lopez, A., Fernandez, R. P.,  
Tilmes, S., Emmons, L. K., and Lamarque, J.: Ocean Biogeochemistry Control on the Marine  
Emissions of Brominated Very Short-Lived Ozone-Depleting Substances: A Machine-Learning  
Approach, *J. Geophys. Res. Atmos.*, 124, 12319–12339, <https://doi.org/10.1029/2019JD031288>,  
2019c.
- 1080 Wang, S., Apel, E. C., Schwantes, R. H., Bates, K. H., Jacob, D. J., Fischer, E. V., Hornbrook, R. S.,  
Hills, A. J., Emmons, L. K., Pan, L. L., Honomichl, S., Tilmes, S., Lamarque, J., Yang, M.,  
Marandino, C. A., Saltzman, E. S., Bruyn, W., Kameyama, S., Tanimoto, H., Omori, Y., Hall, S.  
R., Ullmann, K., Ryerson, T. B., Thompson, C. R., Peischl, J., Daube, B. C., Commane, R.,  
McKain, K., Sweeney, C., Thames, A. B., Miller, D. O., Brune, W. H., Diskin, G. S., DiGangi, J.  
P., and Wofsy, S. C.: Global Atmospheric Budget of Acetone: Air-Sea Exchange and the  
Contribution to Hydroxyl Radicals, *J. Geophys. Res. Atmos.*, 125,  
<https://doi.org/10.1029/2020JD032553>, 2020.



- 1085 Wofsy, S. C., Afshar, S., Allen, H.M., Apel, E.C., Asher, E.C., Barletta, B., Bent, J., Bian, H., Biggs, B.C., Blake, D.R., Blake, N., Bourgeois, I., Brock, C.A., Brune, W.H., Budney, J.W., Bui, T.P., Butler, A., Campuzano-Jost, P., Chang, C.S., Chin, M., Commane, R., Correa, G., Crouse, J.D., Cullis, P. D., Daube, B.C., Day, D.A., Dean-Day, J.M., Dibb, J.E., DiGangi, J.P., Diskin, G.S., Dollner, M., Elkins, J.W., Erdesz, F., Fiore, A.M., Flynn, C.M., Froyd, K.D., Gesler, D.W., Hall, S.R., Hanisco, T.F., Hannun, R.A., Hills, A.J., Hints, E.J., Hoffman, A., Hornbrook, R.S., Huey, L.G., Hughes, S., Jimenez, J.L., Johnson, B.J., Katich, J.M., Keeling, R.F., Kim, M.J., Kupc, A., Lait, L.R., Lamarque, J.-F., Liu, J., McKain, K., Mclaughlin, R.J., Meinardi, S., Miller, D.O., Montzka, S.A., Moore, F.L., Morgan, E.J., Murphy, D.M., Murray, L.T., Nault, B.A., Neuman, J.A., Newman, P.A., Nicely, J.M., Pan, X., Paplawsky, W., Peischl, J., Prather, M.J., Price, D.J., Ray, E.A., Reeves, J.M., Richardson, M., Rollins, A.W., Rosenlof, K.H., Ryerson, T.B., Scheuer, E., Schill, G.P., Schroder, J.C., Schwarz, J.P., St.Clair, J.M., Steenrod, S.D., Stephens, B.B., Strode, S.A., Sweeney, C., Tanner, D., Teng, A.P., Thames, A.B., Thompson, C.R., Ullmann, K., Veres, P.R., Vieznor, N., Wagner, N.L., Watt, A., Weber, R., Weinzierl, B., et al.: Atmospheric Tomography Mission (ATom)ATom: Merged Atmospheric Chemistry, Trace Gases, and Aerosols, <https://doi.org/10.3334/ORNLDAAC/1581>, 2018.

Wood, R.: Stratocumulus Clouds, *Monthly Weather Review*, 140, 2373–2423, <https://doi.org/10.1175/MWR-D-11-00121.1>, 2012.

- 1105 Wood, R., Mechoso, C. R., Bretherton, C. S., Weller, R. A., Huebert, B., Straneo, F., Albrecht, B. A., Coe, H., Allen, G., Vaughan, G., Daum, P., Fairall, C., Chand, D., Gallardo Klenner, L., Garreaud, R., Grados, C., Covert, D. S., Bates, T. S., Krejci, R., Russell, L. M., de Szoeko, S., Brewer, A., Yuter, S. E., Springston, S. R., Chaigneau, A., Toniazzo, T., Minnis, P., Palikonda, R., Abel, S. J., Brown, W. O. J., Williams, S., Fochesatto, J., Brioude, J., and Bower, K. N.: The VAMOS Ocean-Cloud-Atmosphere-Land Study Regional Experiment (VOCALS-REx): goals, platforms, and field operations, *Atmos. Chem. Phys.*, 11, 627–654, <https://doi.org/10.5194/acp-11-627-2011>, 2011.

Wu, R., Wang, S., and Wang, L.: New Mechanism for the Atmospheric Oxidation of Dimethyl Sulfide. The Importance of Intramolecular Hydrogen Shift in a  $\text{CH}_3\text{SCH}_2\text{OO}$  Radical, *J. Phys. Chem. A*, 119, 112–117, <https://doi.org/10.1021/jp511616j>, 2015.

- 1115 Yan, J., Jung, J., Zhang, M., Xu, S., Lin, Q., Zhao, S., and Chen, L.: Significant Underestimation of Gaseous Methanesulfonic Acid (MSA) over Southern Ocean, *Environ. Sci. Technol.*, 53, 13064–13070, <https://doi.org/10.1021/acs.est.9b05362>, 2019.

Yang, Y., Wang, H., Smith, S. J., Easter, R., Ma, P.-L., Qian, Y., Yu, H., Li, C., and Rasch, P. J.: Global source attribution of sulfate concentration and direct and indirect radiative forcing, *Atmos. Chem. Phys.*, 17, 8903–8922, <https://doi.org/10.5194/acp-17-8903-2017>, 2017.



- 1120 Ye, Q., Goss, M. B., Isaacman-VanWertz, G., Zaytsev, A., Massoli, P., Lim, C., Croteau, P., Canagaratna, M., Knopf, D. A., Keutsch, F. N., Heald, C. L., and Kroll, J. H.: Organic Sulfur Products and Peroxy Radical Isomerization in the OH Oxidation of Dimethyl Sulfide, *ACS Earth Space Chem.*, 5, 2013–2020, <https://doi.org/10.1021/acsearthspacechem.1c00108>, 2021.
- 1125 Zaveri, R. A., Easter, R. C., Fast, J. D., and Peters, L. K.: Model for Simulating Aerosol Interactions and Chemistry (MOSAIC), *J. Geophys. Res.*, 113, D13204, <https://doi.org/10.1029/2007JD008782>, 2008.
- 1130 Zaveri, R. A., Easter, R. C., Singh, B., Wang, H., Lu, Z., Tilmes, S., Emmons, L. K., Vitt, F., Zhang, R., Liu, X., Ghan, S. J., and Rasch, P. J.: Development and Evaluation of Chemistry-Aerosol-Climate Model CAM5-Chem-MAM7-MOSAIC: Global Atmospheric Distribution and Radiative Effects of Nitrate Aerosol, *J Adv Model Earth Syst*, 13, <https://doi.org/10.1029/2020MS002346>, 2021.
- Zawadowicz, M. A., Suski, K., Liu, J., Pekour, M., Fast, J., Mei, F., Sedlacek, A. J., Springston, S., Wang, Y., and Zaveri, R. A.: Aircraft measurements of aerosol and trace gas chemistry in the eastern North Atlantic, *Atmos. Chem. Phys.*, 21, 7983–8002, 2021.
- 1135 Zhu, L., Nicovich, J. M., and Wine, P. H.: Temperature-dependent kinetics studies of aqueous phase reactions of hydroxyl radicals with dimethylsulfoxide, dimethylsulfone, and methanesulfonate, *Aquatic Sciences - Research Across Boundaries*, 65, 425–435, <https://doi.org/10.1007/s00027-003-0673-6>, 2003.
- 1140 Zhu, L., Nenes, A., Wine, P. H., and Nicovich, J. M.: Effects of aqueous organosulfur chemistry on particulate methanesulfonate to non-sea salt sulfate ratios in the marine atmosphere, *J. Geophys. Res.*, 111, D05316, <https://doi.org/10.1029/2005JD006326>, 2006.